Prediction of Surface Roughness of Additively Manufactured Parts Using A Photopolymerization Model

By

Ishan Mukund Bhalerao

A thesis submitted to the

School of Graduate Studies

Rutgers, The State University of New Jersey

In partial fulfillment of the requirements

For the degree of

Master of Science

Graduate Program in Mechanical and Aerospace Engineering

Written under the direction of

Howon Lee

And approved by

_____

_____

_____

New Brunswick, New Jersey

October 2018

ABSTRACT OF THE THESIS

Prediction of Surface Roughness of Additively Manufactured Parts Using A Photopolymerization Model

By

Ishan Bhalerao

Thesis Director

Dr. Howon Lee

Additive manufacturing (AM) is a set of processes that build a three-dimensional part by additively joining raw material in a layer-by-layer fashion. This layer-by-layer approach inherently results in a 'staircase', which is prominently observed on the surface of the printed part giving rise to surface roughness. To obtain high quality 3D printed part, post-process finishing techniques are required that adds to high cost and production time. It is a high priority to obtain high-quality parts with minimum post-processing to reduce printing cost and time. In this work, we investigate the effect of printing process parameters on the resulting surface profile through numerical simulation in order to

improve surface quality of the printed part. We use Projection Micro Stereolithography (PμSL) as a model AM process.

A mathematical model based on photopolymerization principle is established to simulate 3D printing environment. This model will produce a layer profile computationally, which is equivalent to experimentally printed layer profile. The shape of the layer is dependent on various printing parameters, including resin constituents such as photo-initiator and photo-absorber, process parameters such as layer thickness and curing time, and environmental factors such as oxygen concentration. The objective of this work is to optimize the process parameters for fabricating high surface quality structures. Varying these parameters will affect the shape of layer and, as a result, surface roughness of the structure as well. Based on the simulated layer profile, a stacked layer structure is generated computationally, from which a simulated surface profile is extracted. This is compared to the experimentally obtained value from a printed part.

Based on Taguchi Design of Experiment method, the number of simulations to be performed is reduced from 3^5 to 27 simulations to achieve minimum surface roughness obtainable within the given range of printing parameter space. The optimized parameters are used to print high quality structures for two different cases. First, vertical micro-struts are printed with optimum parameters and compared with the result obtained with nominal parameters. The result shows that the optimized parameters reduce surface roughness by 40%. Second, simulated micro-struts with an inclination angle are studied as surface roughness increases with decrease in inclination

angle. With the optimized parameters, the simulation shows that surface roughness of the inclined strut decreases by 45% on left edge and 34% on right edge compared to the part with nominal parameters.

In conclusion, surface topography of a vertical or inclined 3D printed strut can be improved by optimizing the print process parameters using the mathematical model and Taguchi method, and high-quality parts can be manufactured with reduced post-processing cost and time.

ACKNOWLEDGEMENTS

I would like to thank my advisor, Dr. Howon Lee, for his continuous support and guidance during the entirety of my research. His support and direction has helped me immensely in the research process.

I would also like to thank the rest of my thesis committee, Dr. Jonathan Singer and Dr. Aaron Mazzeo for their willingness to join my thesis committee and the time that they took out of their schedules to review my thesis.

I would also like to thank my lab mates. Chen Yang and Daehoon Han. It has been great to work with and learn a lot from them. In addition, many thanks to all the undergraduate students working in our lab who have made my time in the lab a fun experience.

Most importantly, I would like to thank my parents for their constant support throughout my college education. They have been amazingly supportive throughout this whole process, and I would not be able to have completed my college education without their help.

In addition, I would like to thank TRUMPF Photonics where I was able to learn about simulations and their importance in research and development of additive manufacturing.

Contents

List of Illustrations

List of Tables

1. Introduction

1.1 Background:

1.1.1 Additive Manufacturing:

Additive manufacturing (AM) is a set of manufacturing processes that utilize additive method to form an object. An additive method is addition of only the required material to fabricate a part. It differs from traditional subtractive manufacturing processes which rely on large material removal to form a part. A layer-by-layer approach is used to successfully fabricate a part as designed on a computer aided design (CAD) software. AM has revolutionized manufacturing industries that take advantage of such processes. Traditional subtractive manufacturing processes use different machines such as computer numeric code (CNC) machines, milling machines etc., that have limitations of producing complex, micro parts because extensive machining is required which is a time consuming and costly process. Research in additive manufacturing has led to equipment development that can readily 'print' complex assemblies, in a single printing process, to significantly cut cost of prototyping.

AM was first introduced in early 1980s and substantial research in the field has led to development of different additive processes that has allowed the use of this technology in many fields [1]. Over the years, AM has found major applications in customizing healthcare products to improve population health and quality of life, reducing environmental impact for manufacturing sustainability and simplification of supply chain to increase efficiency and responsiveness in demand fulfillment.

AM can print structures in macro as well as micro scale. Major research is actively done to produce excellent quality micro parts. AM technologies such as stereolithography (MSL: for micro-stereolithography), selective laser sintering (MLS in microscale), inkjet printing processes, fused deposition modeling (FDM) and laminated object manufacturing (LOM) show promise for developing complex 3D macro and micro parts [1]. Out of all the AM technologies, MSL has proven to be better to producing micro parts because most of the other technologies have been better suited for macro scale fabrication [1].

1.1.2 Projection Micro Stereolithography (PμSL):

The need to manufacture micro objects is seen in important fields such as the bio-medical, robotics and dental industries [1]. The intricate structures can also be manufactured as soft robots capable of locomotion using electroactive hydrogels [14] . Such applications make the technology extremely important for fulfilling the criteria of individualization, function integration, and miniaturization.

Put forth by Suzumori et al. in 1994 [1], PμSL was then a complex and costly system because of the use of physical masks. This mask based MSL method works on the principle of photopolymerization. The main system has five sub-systems that are integrated together. An UV curable resin vat placed on motorized translation stage sits below a projection lens that projects light on the resin in the vat. A UV light source and the mask that can generate the layer pattern to be printed completes the basic PμSL system. In this way, when the UV patterned light is projected on the liquid resin surface,

it undergoes photopolymerization, i.e., it crosslinks and polymerizes, thus forming a layer of the desired shape.

The use of physical masks to generate a pattern required multiple masks to fabricate a part which added the costs. To reduce costs, a dynamic mask was constructed that would eliminate the need of using multiple masks. The dynamic mask would create projection pattern electronically and it was reusable. As presented by Bertsch et al. in 1997, the idea of using liquid crystal display (LCD) as a mask was devised [1]. In 2000, a thin film transistor LCD was used by Hatashi in a PμSL system [1]. LCD masks consists of array of light valves that were made with liquid crystal material. They could be used as the projectors because they were easy to align and cost less, making the system easier and faster to use.

However, the major limitation for using LCD as a mask is more light absorption by the mask when UV light falls on it, thus restricting the resin options that could work effectively with it [1]. As the technology advanced, further limitations were recognized. These include large pixel size corresponding to larger resolution, low switching speeds (speed required to switch to next layer pattern input), and low optical density during OFF mode hinder the contrast of the transmitted pattern [1]. It was Bertsch's research group which suggested the use of digital micromirror device (DMD) by replacing the LCD [1]. In 2005, Sun et al. put forth a system that uses a DMD as a mask generator.

Use of DMD masks simplifies complex part generation by reducing the necessity to rely on LCD screens for UV projection [1]. DMD can be used for most of the UV curable resins, has lower pixel size giving higher resolution, a higher optical density giving

superior contrast of transmitted pattern and higher switching speed. Developed by Texas Instruments®, DMD is a semiconductor chip that has approximately 1.5 million micromirrors stacked in a matrix and mounted on hinges that have size corresponding to the each micromirror [22]. DMD device is capable of producing dynamic pattern due to its high resolution and contrast [1].

A highly advanced PμSL system based on SLA, developed by Yang et al. using DMD is shown in Figure 1.1. A 3D CAD model is designed on computer. The model is converted to a standard tessellation language (*.stl*) format and then the entire structure is sliced, which is converted to a format recognized by the 3D printer. This slicing step converts the *.stl* model into a series of 2D bitmap images each corresponding to a layer that will be 3D printed. This bitmap image is displayed on the DMD. UV light source, usually a UV lamp, is illuminated on the DMD that generates the light pattern of the sliced image displayed on it. This patterned light passes through a reduction lens and is projected on the surface of the resin with a reduced feature size. As soon as the light is incident on the surface of the resin, photopolymerization is initiated forming the layer on a z-axis translation stage. It lowers after the layer is formed and refreshes the resin surface for the next layer to be formed. This process continues until the final structure is formed.

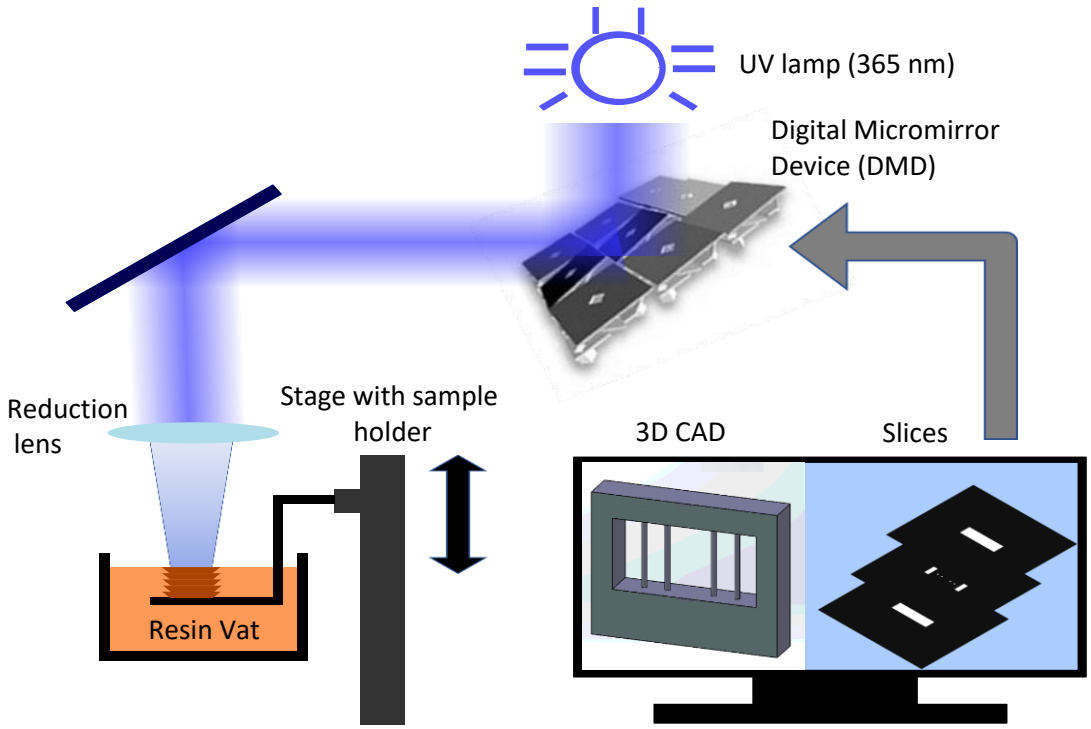

Figure 1.1: Schematic diagram of PμSL

Since 2005, various PμSL systems have been designed to 3D print micro parts. As it requires less time to print a structure, using DMD was a breakthrough in 3D printing industry. Ha et al., in 2008, established a PμSL system that can mass produce microstructure arrays [2]. They developed the system by mounting the optical system on the x-y stage because fabricating arrays will require the patterned light to move on the surface. In 2012, Zheng et al., expressed the limitations of using DMD as a dynamic mask [3]. Since the DMD is an array of micro mirrors, using it in environment prone to dust particles will damage the device, thus making the system unusable. As DMD can efficiently be used only in clean room, they proposed the use of liquid crystal on silicon (LCoS) as the dynamic mask. LCoS chip have highly reflective surface coated with liquid

crystals which provide high contrast ratio, small pixel size and adequate switching speed.

Since PμSL forms a convenient system to develop micro structures, extensive research is done to study how high-quality 3D printed parts can be fabricated.

The challenge in printing is due to the layer-by-layer part formation. This leads to rough surfaces and structures that can have different geometrical dimensions than their CAD counterparts. To address the surface roughness issue, the printed part is subjected to surface finish post-processing which adds to the fabricating cost. This challenge is faced throughout the AM techniques including PμSL. PμSL follows principle of photopolymerization. This chemical process is largely affected by a number of factors including the composition of resin itself to the presence of oxygen in the surroundings. This process can be monitored by understanding the physics behind it and developing a mathematical model. Using this model, the challenge to obtain high-quality 3D printed parts is addressed by creating a simulation to study the 3D printed part. Thus, using the simulation tool to pre-process the printing parameters to their optimal levels to obtain high-quality 3D printed parts having minimum surface roughness reduces the dependency on post-processing techniques.

1.1.3 Mathematical Model: Previous Works

The underlying physics can be studied using partial differential equations that represent the chemical reactions occurring during photopolymerization. Efforts for developing a mathematical model for photopolymerization can be found as early as 1979 by Tryson et al. [4]. A mathematical model put forth by Fang et al describes the

photopolymerization process via a set of coupled differential equations as explained in section 2.1 [5]. They described how including the diffusion term in equations allows proper representation of monomer conversion once the mathematical model is simulated. Inhibition of oxygen has always been a concern in photopolymerization process and Decker et al. in 1985 calculated the value of steady state oxygen concentration of dissolved oxygen at which photopolymerization takes place [6]. It also established the importance of rate constant of propagation (k_p), termination rate constant (k_t) and oxygen rate constant (k_o) will largely affect the photopolymerization since these three terms take part in propagation, termination, and inhibition phase, which is responsible for radical formation as explained in section 2.1.

O'Brien et al studied the impact of oxygen on photopolymerization kinetics and polymer structure [7]. They investigated how the conversion ratio is affected by changing layer thickness, light intensity and oxygen concentration. The paper also discussed about formation of tacky layer due to oxygen influence at the interface of resin and surroundings. A simulation was done to validate the proposal. It followed a mathematical model similar to section 2.1.

Dendukuri et al (2008) established an important relation of oxygen inhibition and free particle generation [8]. Free particle generation is another actively researched topic where PμSL is used to generate particles in micron size. They derived an equation for oxygen inhibition following Decker's conclusion. Comparing simulation and empirical data they validated that oxygen also plays a supportive role in 3D printing.

Zao et al. in 2016 used similar model to calculate strength of printed object [9]. In this part-by-part printing method, the first part is polymerized and effect of oxygen is studied when the second part is solidified. The interfacial strength increases as tacky layer from first part had unconverted double bonds react with the second part after it is solidified. Interfacial strength increases with oxygen concentration and that decreasing the PI concentration will also increase the strength.

Along with model development, extensive research has been done to find results that relate to understanding how the parameters affect the overall printing. Focusing on simulations that have assumptions such as pre-polymerized layer acting as lens for tracing the polymerized profile by Ikuta et al. or using UV light energy deposition method to determine polymerized profile by Nakamoto et al. fall short of results that require analysis of kinetic parameters and importance of each parameter that influences the photopolymerization process [10]. A mathematical model developed by Racz et al. explained photocure kinetics but it did not explain simulation results that obtain an optimized selection of parameters for 3D printing a part [10]. Most of these studies were for macro-scale parts but the micro-scale photopolymerization was recently developed.

The photopolymerization mechanism for micro-scale parts follows a similar mathematical model as for macro-scale parts. A study performed by Xi gives a comparison for macro-scale and micro-scale numerical simulation [10]. The mathematical model explains each of the component in detail and the simulation results that are carried out using numerical methods explains how differently the parameters

behave when considering the scale. For example, the heat generated during a micro-scale printing is extremely low, and can be neglected, but heat generation in macro-scales have a significant impact on photopolymerization components.

1.1.4: Surface Roughness of 3D Printed Structures:

As stated earlier, it has always been in interest to make additively manufactured parts having high quality and match closely with their CAD counterparts. But the layered approach gives rise to challenges such as the 'staircase' effect, also seen in Figure 1.2. Efforts have been taken to understand the factors that affect the surface roughness, and majority of research is done to determine the ideal layer thickness to reduce the staircase effect.

Cure depth and curing width are extremely important in surface roughness determination. When UV light is incident on the surface of resin, the area on which it is incident solidifies. Due to parameters related to resin and environment, the surface may not cure exactly as the light falls on it. It can either cure more or less, giving rise to a layer that is either over-cured or under cured.

The mathematical model helps estimate all the values of the parameters and guides to evaluate the curing depth and curing width. In 2011, Jariwala et al. [11] used resources from [6] and [10] to develop a proper oxygen inhibition simulation to study the overall shape of the cured profile. They presented a 2-D domain that can be utilized to investigate how the structure of a cured layer will fabricate. From the simulation result, they obtained the cured profile of a printed layer for different curing times, showing it increases the cure depth. Their simulation, performed with on COMSOL, fell short of

determining the exact changes that occur by changing the parameters. Also, the experiments showed a very different cured profile and there was no suggestion for surface roughness, yet it is helpful to comprehend that the simulation will offer a good visual of the fabricated layer profile.

Another study done by Ahn et al. in 2009, predicts the surface roughness value after the part is printed [12]. An interpolation equation to determine the surface roughness is introduced and an application is developed on Visual C++ for predicting surface roughness values for 3D printed structures. It gives an understanding on how to extract surface roughness over varied surface angles and how surface roughness can be predicted for a structure. However, it does not take into consideration any mathematical model for photopolymerization parameters or investigate their effects on surface roughness.

An interesting study done by Sager et al. [13] uses a parameter estimation (PE) method to improve surface quality in stereolithography. In this PE method, the surface of interest (surface whose roughness is to be improved) is expressed as a grid, along which the exposure value of light intensity should be equal to critical exposure. By specifying the shape and length of the grid, the surface finish of the cured shape can be controlled. Though the surface roughness was controlled, the limitation for this approach is that if the part is complex, or has many layers, which affects the length, the surface roughness cannot be easily controlled. In addition, using the PE method requires estimation as to decide at which spot in the resin vat should light be shined to achieve the desired surface roughness.

From the various research articles, it is evident that surface roughness control by pre-processing of printing parameters is not completely studied and active research is still being done to either control the surface roughness or to monitor it. This research combines the mathematical model and the surface roughness study to estimate ideal printing parameters to have better surface finish of the 3D printed part.

1.2 Motivation:

The main objective of this research is to identify optimal printing process parameters using a computational model for fabricating high-quality 3D printed structures that can be printed using PμSL. A 3D printed part is a stack of multiple layers each having a definite cure depth. The texture of the part is easily recognizable either by touch or mere observation which can be rough and have dimensions deviated from the original CAD model. To minimize the surface roughness and the variance of the printed part from CAD model, the parameters that affect the printing quality should be studied. The Figure 1.2 shows the expected 3D printed structure and how it may be printed if the process parameters are not controlled. However, using a trial and error method for obtaining high quality parts is a long process since it requires multiple time-consuming experiments.

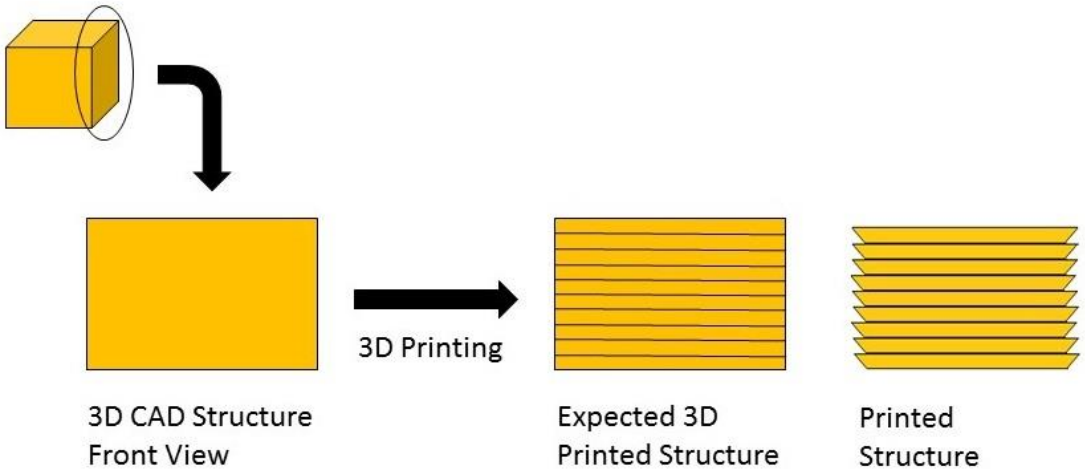

Figure 1.2: Expected and actually printed 3D structure representation

The printing process parameters are a combination of resin composition, environmental oxygen, and experimental input parameters. They are identified using the mathematical model and experimental validation and their effect on layer structure is studied. This classification allows to design the experiment by shortlisting the factors that would result in rough surface.

Thus, by creating the simulation, one can predict how the 3D printed structure's side profile will form. To fulfill this requirement, it is important to understand the mathematical model, how it is used to develop simulation, and how it can be validated before been deployed.

Taguchi Analysis is used to reduce the number of simulations to be performed for giving robust result, i.e. high-quality 3D printed parts. This method ensures the selection of optimal printing process parameters. Using this method will aid to select optimal

parameters for the resin, reduce time consumed in material selection, enhance quality of 3D printed parts and act as a reference to investigate different types of resins.

1.3 Thesis Organization:

Firstly, the mathematical model is developed based on the research guidelines from [6] to [13] in Chapter 2 along with experimental set up. The model is validated using empirical data performed on PμSL apparatus, which will be explained in Chapter 3. An estimation of curing width and curing depth is developed from the validation. The model is analyzed on COMSOL and results are documented that show the variation in curing depth and width for different experimental parameters.

Chapter 4 begins with surface roughness profile measurement from the empirical and computational data. To find optimal parameters, Taguchi analysis is performed and the result is studied using simulation data. The optimized parameters are investigated by experimental validation to prove that the selected parameters will help in achieving high-quality 3D printed structures. Summary and future work is discussed in Chapter 5.

2. Materials and Methods

2.1 Computational Model

2.1.1 Principle of Photopolymerization

A photocurable resin, which can undergo photopolymerization due to free radicals, can be explained using three steps [15] . Initiation, propagation, and termination. Oxygen concentration in the surrounding plays an inhibitive role in photopolymerization. The concentrations of each constituent in the resin may vary depending on the application, and such specific resins can be prepared in a laboratory. The photo initiators are UV sensitive and therefore UV light is used in the setup. When UV light is projected on the resin, active radicals are generated from the photoinitiator. The active radicals readily react with the monomer molecules, which cross-links the monomers to form polymer chains. This propagation of cross-linked polymer chains continues until a larger polymer is formed. When two large chains of polymers cross-link with each other, the reaction terminates and the resulting structure is the solidified polymer structure, often known as a ‘layer’ of photocured resin, as shown in Figure 2.1.

(a)

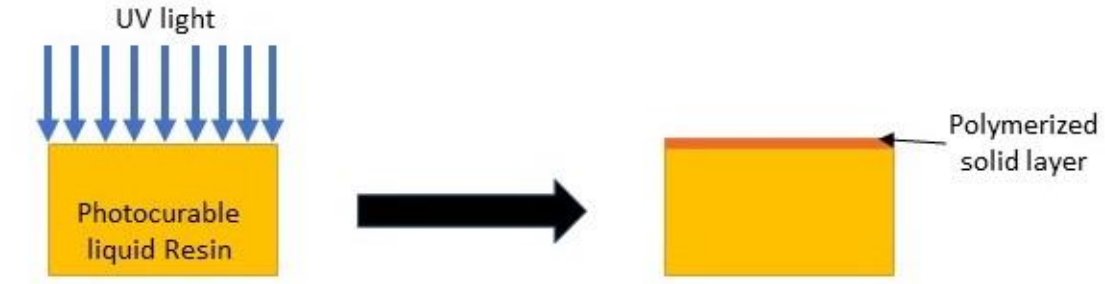

(b)

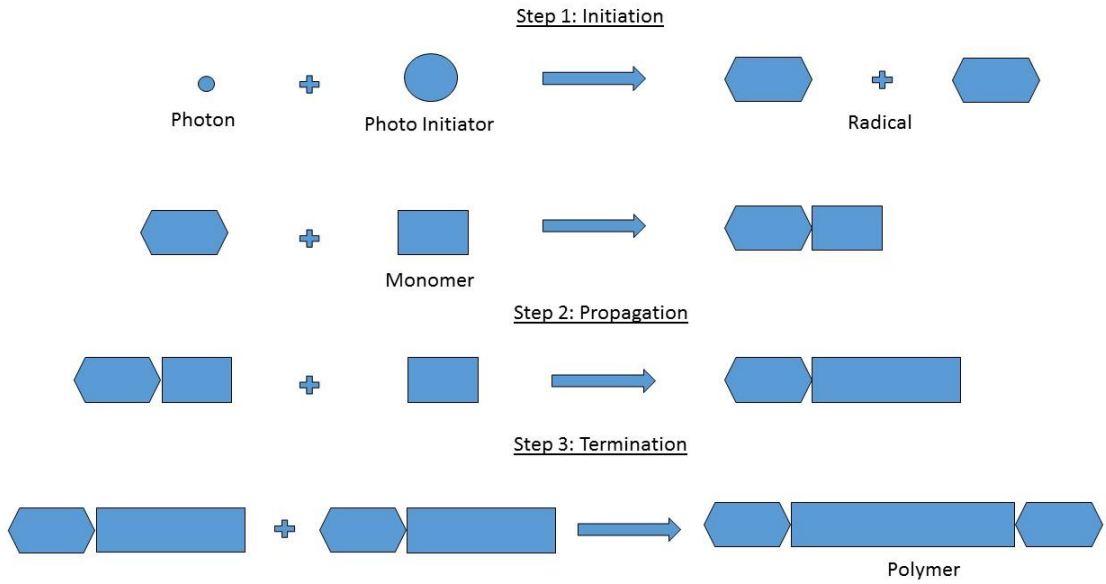

Figure 2.1 (a) Photopolymerization principle (b) Illustration of reaction process

An important factor that plays vital role in the radical concentration determination is actually an environmental parameter in the photopolymerization reaction. Oxygen concentration in air acts an inhibitive agent in the photopolymerization process, which forms the fourth part of the photopolymerization process. Radicals at the interface between resin and air not only react with monomer molecules, but also react with

oxygen molecules in the air, by forming peroxides. These peroxides no longer take part in the polymerization process, thereby inhibiting the overall conversion of resin from liquid to solid.

2.1.2 Photopolymerization Model

At the surface of the resin, the light is absorbed. This projected light or light intensity (I) absorption in resin, which is given by

$$\frac{dI}{dz} = -(\alpha[PI] + \alpha_a[PA])I \qquad (2.1)$$

In equation 2.1, [PI] and [PA] represent photoinitiator and photo absorber concentrations, *I* is the light intensity, α is molar absorptivity of photoinitiator and α_a is the molar absorptivity of photo-absorber [5]. It establishes the initiation phase of photopolymerization. The term $'(\alpha[PI] + \alpha_a[PA])'$ represents the absorption coefficient 'A', which follows the Beer-Lambert law. Ideally, the absorption terms include photoinitiator, photo-absorber, monomer, reactive polymer chains with various weights, and terminated polymer materials. However, for UV polymerization these proportions are difficult to determine because of their concentrations and molar extinction coefficients are not monitorable with no equipment available in the lab to measure them [10]. It can be said that primarily, [PI] and [PA] are assumed to be the major absorbents in the resin and are therefore considered in equation 2.1.

UV projection on resin surface ideally should be represented by a step function, i.e. a top-hat function. However, this ideal projection pattern is not achieved because as the UV light passes through the optical elements, the loss in sharpness needs to be accounted and that results in a Gaussian-shaped projection. This is characterized by

modulation transfer function in frequency domain and point spread function in spatial domain [17]. The ideal pattern and the actual projected pattern of light falling on the fabrication surface is shown in Figure 2.2.

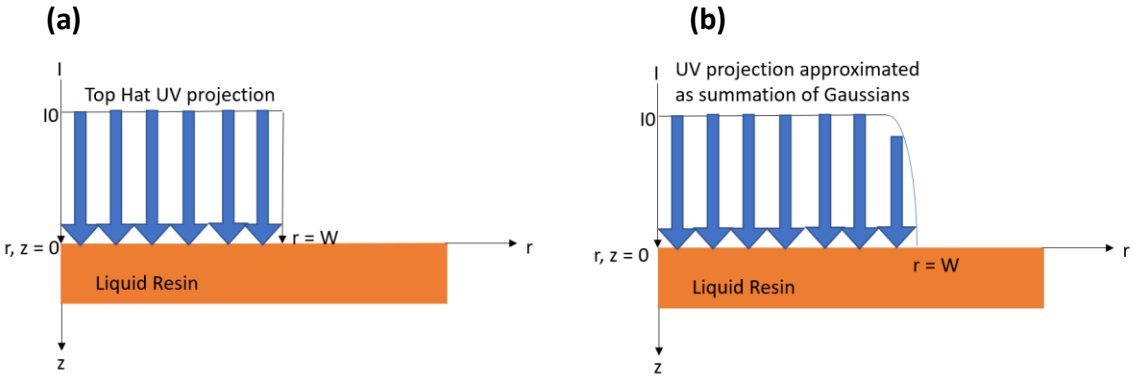

Figure 2.2 (a) Schematic of ideal or expected projection. (b) Actual projection due to blurriness introduced by optical system

The Gaussian distribution pattern is represented for beam width corresponding to resolution. Because of this, a summed Gaussian function is expressed below. The summed Gaussian will represent number of pixels projected on surface of resin, each pixel having a resolution in microns, thus representing the actual projection. In the equation 2.2, '*w*' is the beam width if beam is for a single pixel, which corresponds to the resolution of a single pixel, '*n*' is the number of pixels, 'I_0' is the peak light intensity and r is the radial direction representing the surface of the resin. For n number of pixels, the light intensity equation is given by 2.3.

$$I = I_0 * e^{\frac{-2(r)^2}{w^2}} \tag{2.2}$$

$$I = I_0 * \sum_0^n e^{\frac{-2(r-\mathbf{w}*\mathbf{n})^2}{w^2}} \tag{2.3}$$

As explained in the photopolymerization principle, under the influence of UV light, the photoinitiator molecules split into radicals. Due to this, PI concentration will decrease. This is known as consumption of photoinitiator and its rate can be written as [5]

$$\frac{\partial[PI]}{\partial t} = \nabla(D_{PI}\nabla[PI]) - \frac{1}{2}\phi\alpha\beta[PI]I \tag{2.4}$$

Equation 2.4 introduces the diffusion term of D_{PI} since the projection of the UV light will create a concentration gradient of photo-initiators as well as radicals. This gradient will drive the molecules diffusing from high concentration region to low concentration region, that will result in mass transfer. Coefficient 'ϕ' is the quantum yield of radicals, i.e., the number of photoinitiator molecules photolyzed by one actinic photon of UV light. β is the value that is derived from quantum yield. Since,

$$\phi = \frac{\text{Number of molecules decomposed}}{\text{Number of photons absorbed}} \tag{2.5}$$

So, as the governing equation for photoinitiator is in unit mole, the unit of denominator is in Einstein, which is total energy of one mole of photons. For monochromatic light with 365 nm wavelength, 1[Einstein]= 2.7217e5[J] [18]. Thus,

$$\beta = \frac{1}{3.27e5}$$

The moment the patterned UV light falls on the resin, the photoinitiator molecules split to form radicals. Each photoinitiator molecules generates 2 radicals.

As soon as the radicals are generated, they react with monomers and activate their functional groups. These active monomers react with other monomers that begins a propagation reaction [10], given by

$$\frac{\partial[M]}{\partial t} = -k_p[M][R] \quad (2.6)$$

Where [M] is the monomer concentration, k_p is the propagation rate constant and [R] is radical concentration. Since equation represents consumption of monomer concentration, a negative sign is added in the equation, indicating that the monomer concentration should decrease as photopolymerization progresses. The radical concentration should be estimated as well. The generation and consumption of radicals can be explained with the help of following terms

$$R_g = \phi\alpha\beta[PI]I_0 \exp(-\alpha[PI]z) \quad (2.7)$$

$$R_c = k_t[R]^2 + k_o[O][R] \quad (2.8)$$

Here, R_g and R_c are the radical generation and consumption terms. [R] is the sum of all the types of radical species formed since it is impossible to separate different radical species in the mixture as their quantities are extremely low [10]. The generation term is proportional to second term of equation 2.4. The consumption term has two parts. The active radicals not only react with monomers, but also with themselves. This is because when they react with active monomers, the monomers react with other monomers to form polymers. This represents the crosslinking phenomenon. As the radicals do not find more monomers to react with, they react with themselves and this in turn reduces the radical concentration, which is represented by the squared radical concentration term. The second part of the consumption term is because of the oxygen concentration ([*O*]) in air, which acts an inhibitive agent in the photopolymerization process. Radicals at the interface between resin and air not only react with monomer molecules, but also react with oxygen molecules at the surface of resin, by forming peroxides. These peroxides no

longer take part in the polymerization process, thereby inhibiting the overall conversion of resin from liquid to solid.

However, by allowing the process in an oxygen free environment, it is possible to eliminate this inhibitive action. Nonetheless, for this study, radical concentration with oxygen concentration is studied. [O] is the oxygen concentration in the air, k_t is the termination rate constant and k_o is the oxygen rate constant. Radical diffusion (D_r) plays a vital role in the determination of radical concentration. Thus, the radical concentration can be given by the following equation 2.9 [9],

$$\frac{\partial R}{\partial t} = \nabla(D_r \nabla[R]) + \phi\alpha\beta[PI]I - k_t[R]^2 - k_o[O][R] \quad (2.9)$$

Where the first term denotes the radical diffusion term. The oxygen inhibition is given by the equation 2.10 [8]

$$\frac{\partial O}{\partial t} = \nabla(D_o \nabla[O]) - k_o[O][R] \quad (2.10)$$

Where, D_o presents the oxygen diffusion constant. In the above equations there are three rate constants: k_p, k_t and k_o. According to empirical Arrhenius formula, heat transfer equation in process should be considered in case that the temperature rise during the exothermal process cannot be ignored. Since enthalpy will be released during photopolymerization [10], conservation of internal energy is given by,

$$\rho C_p \frac{\partial T}{\partial t} = k\nabla T - \frac{1}{2}\sqrt{\frac{[M]_0}{[M]}}\frac{d[M]}{dt}\Delta H \quad (2.11)$$

Where ρ, C_p, k and ΔH are density of monomer, heat capacity of the monomer, thermal conductivity and calculated heat of 100% reaction respectively. Equation 2.11 is

determined from the following empirical equation for determining the conversion ratio by utilizing the initial monomer concentration $[M]_0$ and [M] after photopolymerization [5]. Conversion ratio (C), which is the output of simulation at each time step, can therefore be determined using,

$$C=1-\sqrt{\frac{[M]}{[M]_0}} \tag{2.12}$$

For simulation purposes, conversion ratio of resin from liquid resin to solid polymer gives tremendous knowledge about the entire process which will be explained in detail in next chapter. Since all these equations are coupled, the value of conversion ratio will be always dependent on the concentrations of all the contributing photopolymerization parameters. This mathematical model will help determine the ideal parameters from the given side profile, or side profile from given parameters.

2.1.3 Implementation of Mathematical Model in COMSOL Multiphysics

COMSOL is simulation software that can integrate different physics together. It can be used to create a domain that mimics the resin in the vat of the PμSL system. This domain is 2D axisymmetric and is represented by a rectangle, which is a cross section of the 3D vat, which is a cylindrical container, as shown in figure 2.3. Here *z* represents the depth direction, *r* is the radial direction that represents the surface of the resin and *I* is the light intensity. The domain is selected in such a way that the light incident on the surface will allow enough area for resin components to diffuse, i.e., the parameter concentrations equations will be able to converge within the refined mesh area of the

domain. This geometry also helps to investigate layer profile at different conversion ratios.

Once the basic geometry is set, the next step is inputting the parameter values. The 2D domain represents the vat area on which UV light irradiates. Comparing this simulation setup with experimental procedure can be explained by resin preparation and placing it into the vat.

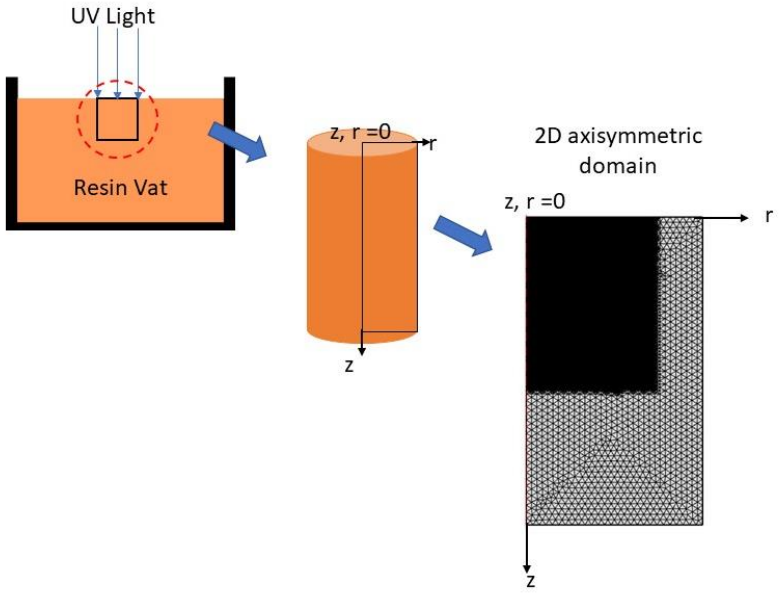

Figure 2.3 2D axisymmetric simulation domain representation of UV induced resin region in the vat.

Setting up the simulation is done in next step by applying the partial differential equations to the domain. They can be represented in COMSOL using the mathematics type of physics which allows full control over the physics selection. As the partial differential equations are convection-diffusion equations, the generalized convection-diffusion mathematics is chosen, which can be modified according to every equation explained above. Since the equations are coupled, COMSOL will automatically solve

them to get value of the terms for each time-step. The equations listed below are used in simulation and table explains the boundary and the initial conditions.

Initiation:

$$\frac{dI}{dz} = -(\alpha[PI] + \alpha_a[PA])I$$

$$\frac{\partial[PI]}{\partial t} = \nabla(D_{PI}\nabla[PI]) - \frac{1}{2}\phi\alpha\beta[PI]I$$

Radical generation or Termination:

$$\frac{\partial R}{\partial t} = \nabla(D_r\nabla[R]) + \phi\alpha\beta[PI]I - k_t[R]^2 - k_o[O][R]$$

Inhibition:

$$\frac{\partial O}{\partial t} = \nabla(D_o\nabla[O]) - k_o[O][R]$$

Propagation:

$$\frac{\partial[M]}{\partial t} = -k_p[M][R]$$

Conversion (Output of each time step):

$$C = 1 - \sqrt{\frac{[M]}{[M]_0}}$$

Table 1 Initial and Boundary Conditions for 2D resin simulation domain

Equation	Initial Condition	Boundary Condition
Initiation: (I)	-	$I(r, z=0) = I_0 * e^{\frac{-2(r-w*n)^2}{w^2}}$
Initiation: [PA]	$[PI]\ (t=0, r, z) = [PI]_0$	-
Termination: [R]	$[R]\ (t=0, r, z) = 0$	$[R]\ (r, z=0) = 0$
Inhibition: [O]	$[O]\ (t=0, r, z) = [O]_1$	$[O]\ (r, z=0) = [O]_0$
Propagation: [M]	$[M]\ (t=0, r, z) = [M]_0$	-
r= radial direction, z=depth direction & t= time		

The initial conditions are the values the parameters will have in the entire domain, while boundary conditions are limited to particular surface of the domain. Figure 2.4 represents the 2D domain and axisymmetric boundaries.

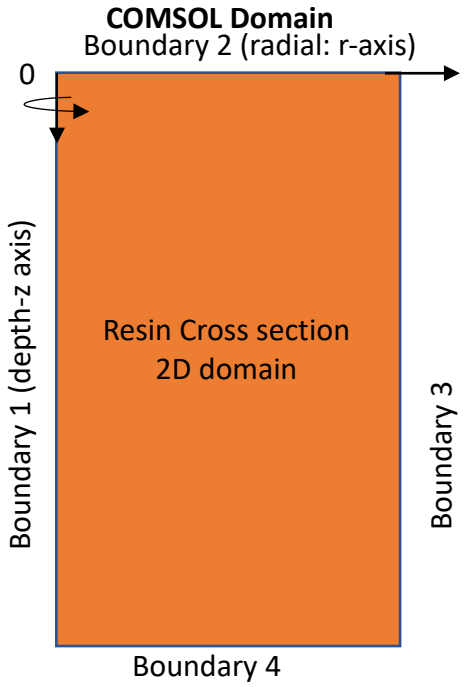

Figure 2.4 COMSOL Domain

Following assumptions are made while setting up the simulation

a) The system is axisymmetric.

b) Thermal properties are considered to be constant in the polymerization reactions. This assumption is made based on analogy that when polymerization on micro scale is limited on a small area, the surrounding resin acts a cold reservoir. In other words, the small heating source is surrounded by a huge cooling system. [10]

c) The rate constants k_t and k_p are kept constant since influence of oxygen (k_o) is considered. k_t and k_p depend on monomer conversion C and influence the

propagation and termination reactions. From experimental data obtained from Tryson et al.'s work [4], fitted curves are generated. For simplification of system, k_p value is assumed to have a higher value, which will be necessary for propagation term to become dominant to initiate radical generation. If it is kept low, the influence of oxygen will be dominant thereby showing no conversion. At the same time, the termination rate k_t is balanced out to a lower value to allow conversion to take place.

d) Optical effects such as refraction or reflection are not considered.

Based on the assumptions, following constants and their values are listed in the table below.

Table 2 List of Parameters

Symbol	Value and [unit]	Parameter Description
W	12[μm]	Gaussian radius
$[M]_0$	4.46e3[mol/m^3]	Monomer initial concentration
$[PI]_0$	48.27[mol/m^3]	Photoinitiator initial concentration
$[PA]_0$	4.06[mol/m^3]	Stabilizer concentration
α	11.9[m^2/mol]	Molar absorptivity of photoinitiator
α_a	4600[m^2/mol]	Molar absorptivity of stabilizer
φ	0.59	Quantum yield for initiator
T0	303[K]	Environmental temperature
D_r	3.0e-10[m^2/s]	Radical diffusion coefficient
D_{PI}	3.0e-10[m^2/s]	Initiator diffusion coefficient
I_0	24.5[mW/cm^2]	Incident light intensity
k_{p0}	25[m^3/mol/s]	Propagation rate constant
k_{t0}	2520[m^3/mol/s]	Termination rate constant
β	1/3.27e5	Amount of energy contained in one photon
t0	5[s]	Time for which light is incident on resin surface
Tlast	0.2[s]	Decay time for the turning the illumination off
Ko	15 [m^3/mol/s]	Oxygen diffusion constant
$[O]_0$	0.9[mol/m^3]	Initial oxygen concentration in resin
$[O]_1$	8.69 [mol/m^3]	Environmental oxygen concentration
D_O	2.84e-11[m^2/s]	Diffusivity constant of oxygen

For any simulation to perform confidently, meshing plays a pivotal role. Meshing the domain is required for accuracy of the result. It is a basic requirement in any FEA analysis. To investigate the accuracy of the mesh, the simulation was set and computed to obtain the result of cure width. The mesh size was refined until accurate value was determined. Since cure width is a known value, the result of the simulation cure width for different refinements of mesh are studied. Since this simulation is time-dependent, it is necessary to analyze the time step as well.

Since the computer would go out of core for mesh refinement beyond 3, a 3 times refined mesh is implemented in the simulations. The time step of 0.1 seconds is used to carry out this time-dependent study.

Now, as the simulation is set up, computational analysis is performed to validate the model and use it for optimizing resin parameters.

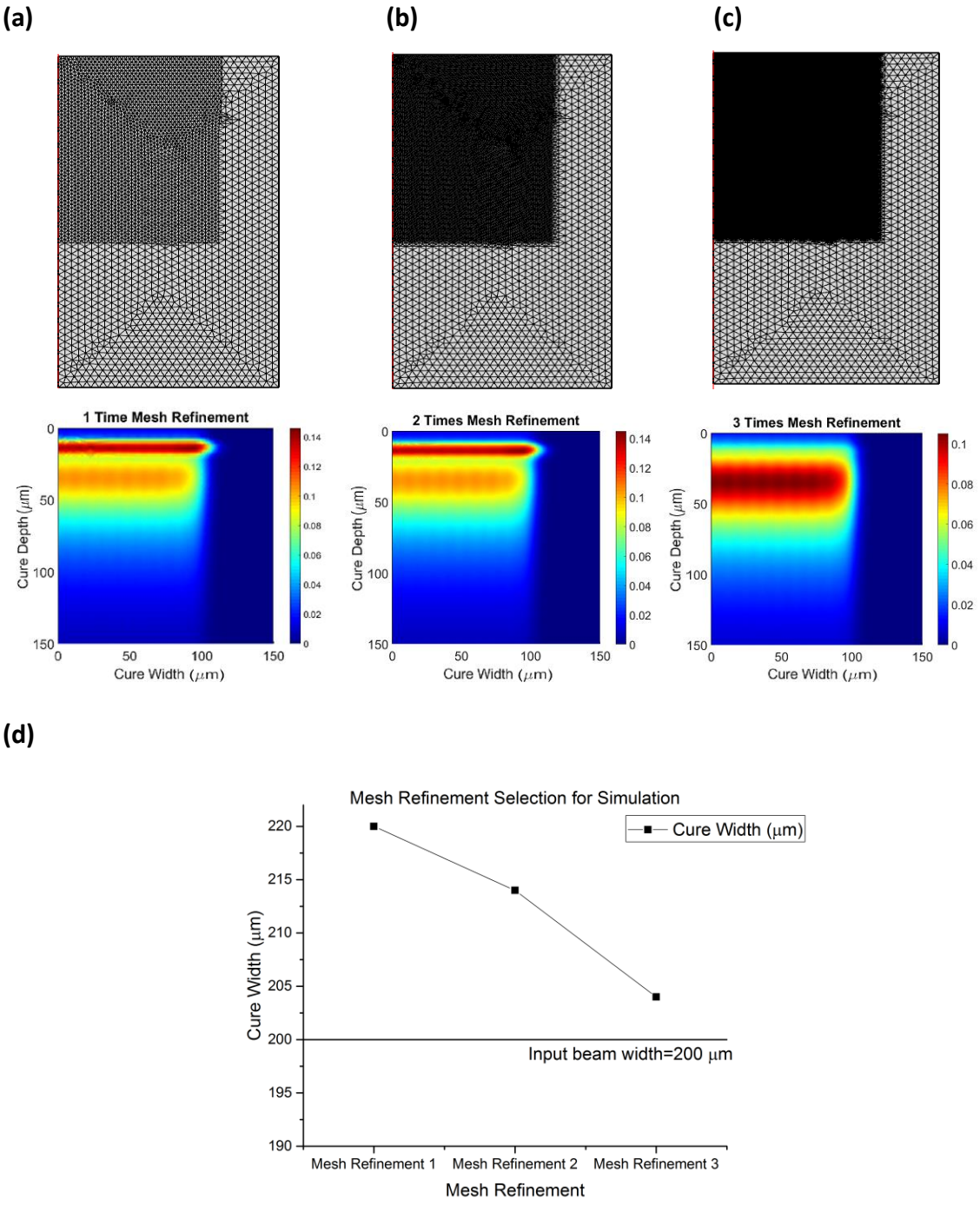

Figure 2.5 Mesh Refinement Analysis. (a), (b) and (c) show refinement of user defined coarse mesh and its impact of the contour plot. The contour plot shows conversion of resin where the red region is resin converted into polymer layer and blue region indicates liquid resin. Each element of the mesh is an equilateral triangle. The quality of the mesh depends upon the skewness of each element. Finer mesh will result in lower skewness and therefore more accurate simulation result. Mesh refinement 3, as seen in (c) and (d) will be able to estimate simulation results close to the input beam width.

Analysis can also be performed using an adaptive mesh. Since the refinement beyond 3 goes beyond available computational power, the study settings in COMSOL can be extended to include time-dependent adaptive mesh. It can significantly further refine already refined mesh to reduce the error. For this case, an adaptive mesh study was performed. The triangular element size for refined area in the mesh represented in Figure 2.5 (c) is about 2 µm which is further refined to as small as 0.5 µm with adaptive meshing. Figure 2.6 shows the adaptive mesh. The cure width value by implementing adaptive mesh was determined. It is observed that adaptively refining the mesh results in cure width value similar to standard three times mesh refinement, which is 205 µm. This can be attributed to the mesh being adapted in z-direction and refinements in r-direction cannot contribute to further convergence because of the use of Gaussian beam convolution. Therefore, mesh in Fig 2.5 (c) is used as the primary mesh for computation because using adaptive mesh increases the computational time and memory usage.

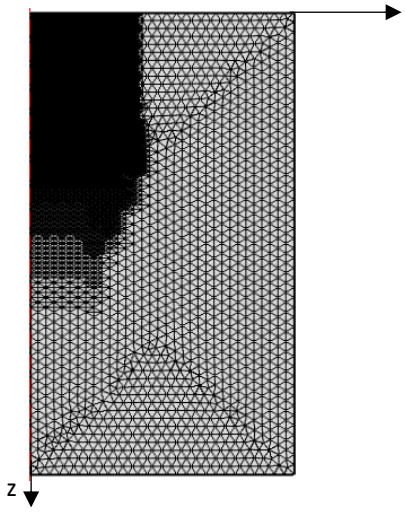

Figure 2.6 Adaptive mesh showing refinements in area where UV light is illuminated. Refinements and asymmetry of the mesh is observed in z-direction.

Based on the mathematical equations, the resin constituents change with time as photopolymerization progresses. To study the changes that take place it is necessary to implement time-dependent computational study. In COMSOL, a time-dependent study will include the start time (t_{start}) of reaction which is 0 seconds while the end of reaction will be the end time (t_{last}). The progression will occur in time steps, which can be set by the user. Different time steps are used to evaluate the performance of the simulation. Figure 2.7 shows effect of varying time steps on simulation result. Cure depth is plotted on y-axis and x-axis represents the energy dose, which is the product of light intensity and time (in seconds) it is exposed on resin surface. The resin parameters used were 2% of [PI], 0.1% of [PA], and 21% of [O]. It can be seen that meshing has a greater influence on simulation result than varying the time step. Based on results, the time step used is 0.1 seconds for all simulations as it will reduce computation time and contribute to result accuracy.

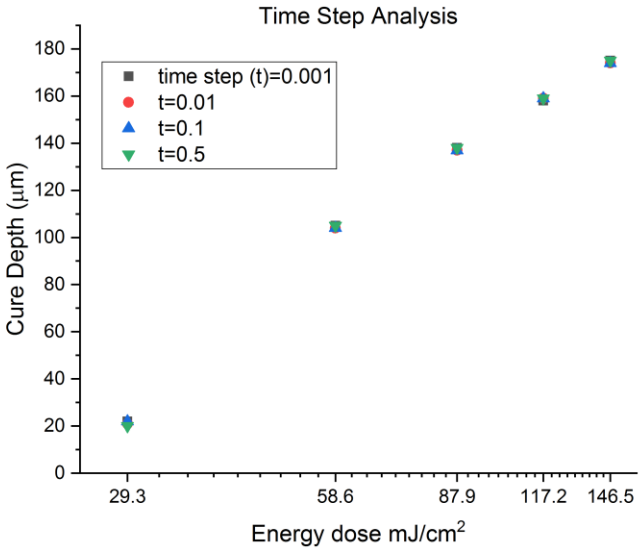

Figure 2.7 Time step analysis shows varying time steps will not affect the simulation accuracy

2.2 PμSL Experimental Set Up

2.2.1 Materials

In the present work, the monomer used was 1,6- Hexanediol diacrylate (HDDA), technical grade 80% (Mol wt. =226.27 g/mol, Sigma-Aldrich now known as Millipore Sigma, St. Louis, USA). The photo-initiator used was Phenylbis (2,4,6-trimethylbenzoyl) phosphine oxide (Mol wt.=418.46) also from Sigma-Aldrich. It is also known by the name Irgacure 819. The photo-absorber used was 1-Phenylazo-2-napththol, also known as SUDAN-1 (Mol wt.= 248.28 g/mol, Sigma-Aldrich). Ethanol was used to wash away excess of resin after photopolymerization. Each sample was placed into ethanol bath for 2 to 3 seconds and an air gun was used to dry the samples.

2.2.2 Experimental Set Up

The system was built by Yang under Prof. Lee's guidance. It is a custom-built projection based stereolithography printing system capable of manufacturing micron sized structures. It consists of a linear stage (cat. No. MTS50-Z8, Thorlabs) [14], on which the sample holder is attached. The sample holder lowers down in the vat filled with resin each time a layer is printed.

A convex lens (convex lens, Thorlabs and extracted lens from commercial digital projector, CANON Realis SX50) is used to achieve the resolution of 12 micron/pixel. The lens is held at an optimal focal length distance of around 5.5 inches to guarantee sharp projection. This ensures that the resolution of 12 microns is achieved.

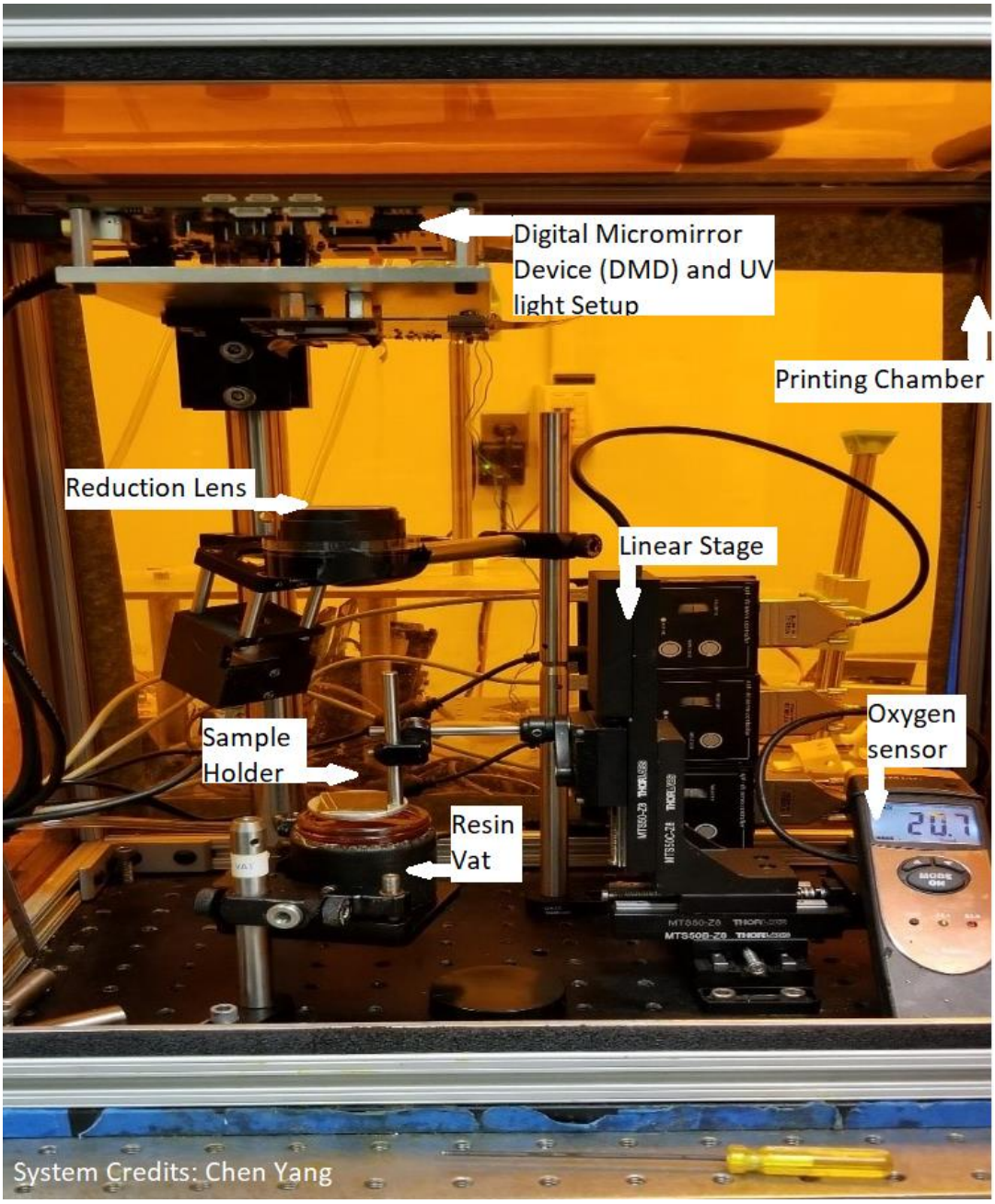

Figure 2.8 Experimental Setup used for 3D printing structures

The digital micromirror device (DMD) (cat. No. DLPLCR6500EVM, Texas Instruments) is used for generating projection patterns according to the sliced images. Finally, UV LED (cat No. L10561, Hamamatsu) with 365 nm wavelength is used for projection. The UV light is reflected from the DMD, which then takes the shape of the patterned layer,

which falls on the convex lens where its resolution is optimized and is projected on the surface of the resin inside the vat on the sample holder that is attached to the linear stage, forming the required layer. The setup is illustrated in the Figure 2.8.

The setup is kept in a printing chamber. The orange color of the chamber walls protects the setup from excess light that may affect printing. The chamber also keeps the system dust free and it can also be used to limit oxygen concentration in the surrounding. The oxygen sensor detects the oxygen concentration in the chamber. Nitrogen gas is pumped in the chamber to control oxygen concentration. The system has the capability of completely eliminating oxygen from the chamber.

2.2.3 Samples for Curing Depth Study

The cure depth study is performed by printing bridge structures. A rectangular layer supported at its two ends is printed which has no supporting layer underneath. This ensures that we can measure the thickness of that particular bridge since the thickness will not be impacted by the layer underneath or above it . A single structure is designed in which the bridges can be printed for different energy dosages at a distance from each other. Each structure has two sets of bridges and each structure is printed twice, thus giving four bridge samples for each set of parameters that are varied. The structures are printed with a notch between two bridge layers. This protruding notch is added at the center of the bridge supports. It is added for the layer thickness measurement purpose. It ensures optimal dimension of the printed bridge.

Figure 2.9 Bridge structure illustration for cure depth measurement

The parameters variation includes PI, PA, Environmental oxygen concentration and curing time. Since the thickness is to be measured, the bridge structures are given zero-micron layer thickness, while the remaining layers are given a layer thickness of 80 microns. After each structure is created, it is placed in ethanol for 2 to 3 seconds and then the excess of resin around the structure is blown with an air gun. This is repeated for every structure. Finally, the measurements are done as explained in section 2.2.4. The following table lists the parameters varied. When one of the parameters is varied, the remaining parameters are kept constant to study the effect of each parameter individually.

Table 3 Printing Parameters for HDDA

Concentration level	Photo-initiator [PI]		Photo-absorber [PA]		Environmental O_2 [O]	
	mol/m^3	%	mol/m^3	%	mol/m^3	%
Low	24.14	1	2.03	0.05	4.14	10
Medium	48.27	2	4.06	0.1	6.21	15
High	72.4	3	6.1	0.15	8.69	21

2.2.4 Curing Depth Measurement

The printed samples are first placed under an optical microscope which has an attached camera. A 5x lens is selected for observing the structures. The stage of the microscope is

adjusted until the bridge layers come into focus which can be monitored using a monitor. A microscope mountable camera is attached to the optical microscope and connected to the computer to allow easy observation. The camera allows to capture the part of the structure which is focused on. The bridge structure for every sample of every structure are captured and stored in computer. To avoid error in focusing on the bridge, the lens is actually focused on the notches in between the bridges that will give the optimal layer thickness of each bridge.

The printed samples are measured for their depth using ImageJ software. Each cure depth is measured at the center of the layer as shown in the figure below. The value obtained from measurement is in pixels and the pixel to microns conversion is done based on the image size and conversion factor. Every image captured from ImageJ has the default size of 1280x1024 pixels, and the conversion factor for 5x optical zoom is 1.265 µm/pixel. Accordingly, each layer's thickness is measured.

(a) **(b)**

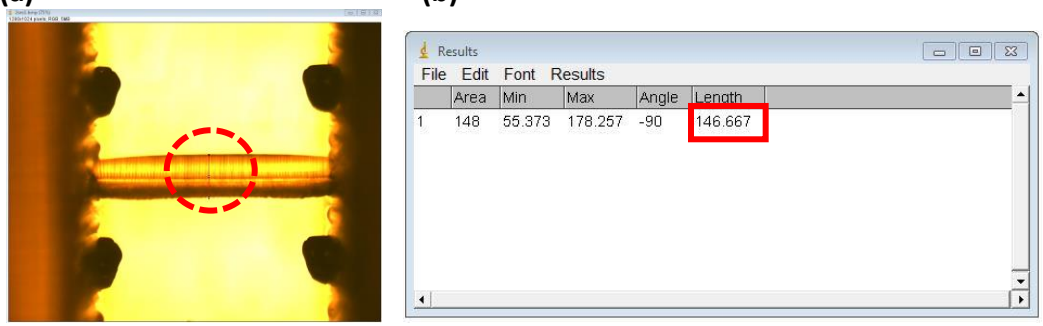

Figure 2.10 (a) Use of ImageJ line tool to measure cure depth. The optical lens is focused on the notches to find optimal depth. (b) Pixel length of line drawn at the center of the layer. Conversion is done to microns based on conversion factor.

2.2.5 Samples for Surface Roughness Study

Surface roughness study is done to obtain high quality parts through Taguchi Analysis. The parts printed are circular struts. A model is developed in SolidWorks as shown below.

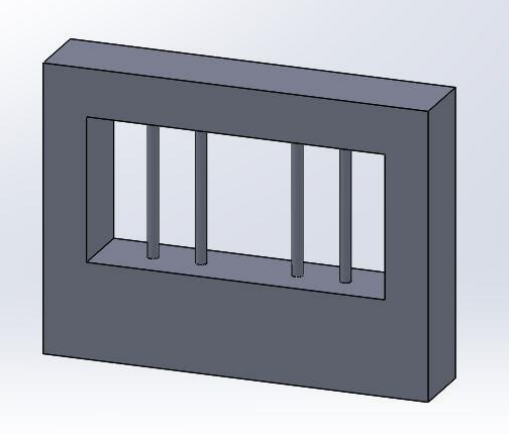

Figure 2.11 SolidWorks Model for printing struts for surface roughness measurement

The model is then converted into *'.stl'* format and is sliced through a slicing software. During slicing, the layer thickness is determined. Parameters are randomly chosen to print a sample and its surface roughness is recorded. Taguchi Analysis is done to find optimized parameters and the selected parameters are used to print a high-quality part. The stark difference in quality of structure is observed. This is explained in detail in Chapter 4.

2.2.6 Surface Roughness Measurement

In most of surface roughness analysis contact method is used to obtain surface roughness data empirically. This often damages the part structure and may cause error in measurement. In this work, image analysis is used to measure the surface roughness of the printed struts. Image of the strut is captured through the camera mounted on the

optical microscope. The edge profile from the image is extracted and is used to find the surface roughness.

3 Model Validation

This chapter focusses on estimation of cure depth and cure width by studying how each experimental parameter affects it. The experimental cure depth data is compared with simulation data to validate the model. Effect of each parameter is evaluated after the simulation model is validated with the help of experimental data.

3.1 Working Curve and Characteristic Values:

When a beam of light with beam width of *w* falls on the surface of the resin, it solidifies to a certain depth. This depth, as explained earlier is the cure depth or C_d. Equation 3.1 determines the curing depth can be expressed as [15]:

$$C_d = D_p \ln\left(\frac{E_{max}}{E_c}\right) \tag{3.1}$$

The above equation introduces D_p as the penetration depth, E_{max} as the maximum exposure and E_c as the critical exposure. From the equation, it is seen that cure depth is proportional to natural logarithm of the maximum exposure. When a plot is generated with E_{max} on x-axis and C_d on y-axis, where x-axis has a log scale, it should be a straight line. This is known as the working curve [15] for a given resin. D_p is the slope of the working curve and E_c is the *x* intercept. Theoretically, the cured depth is 0 at E_c, but it indicates that if exposure is less than the value of E_c, then photopolymerization will not take place. This characteristic value is also the gel point of the resin. Since the research focuses on curing depth and cure width of the printed part, it is necessary to establish working curves to evaluate through experiment and simulation.

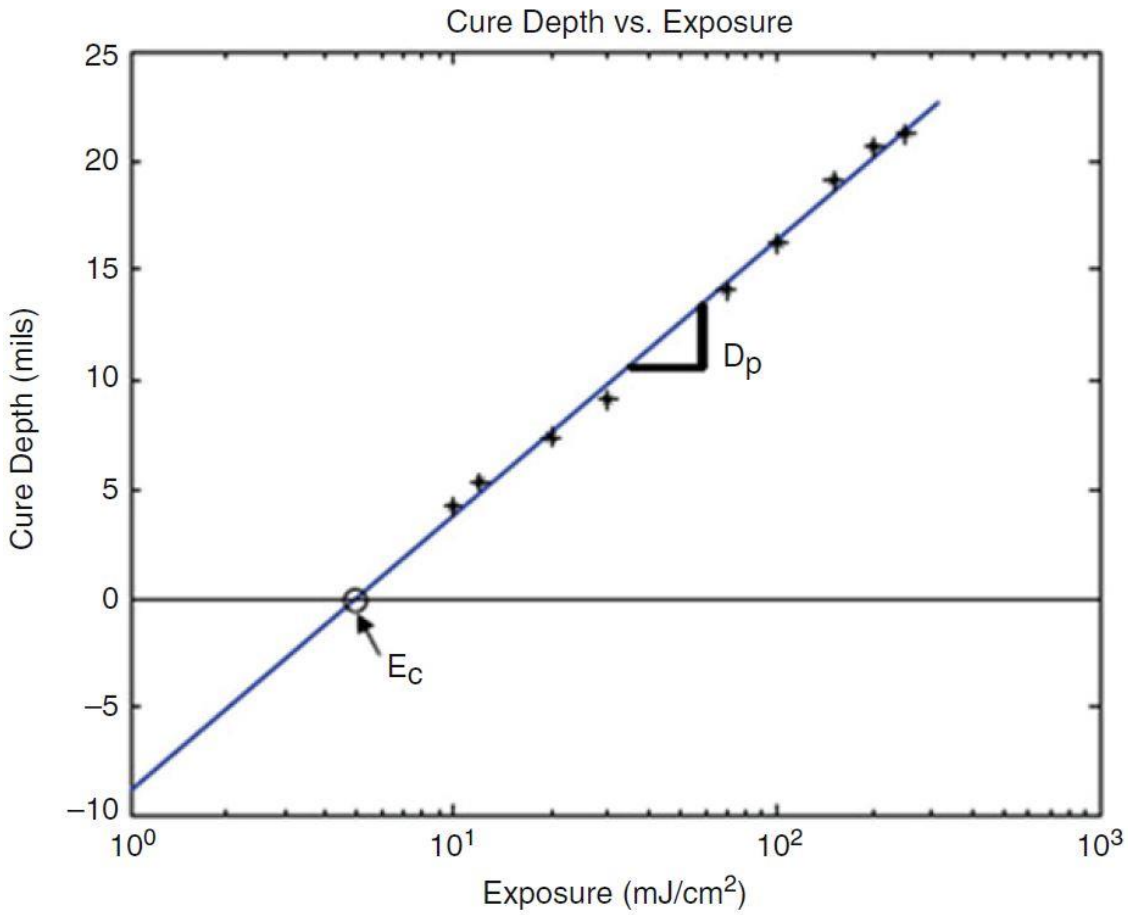

Figure 3.1 Working Curve for determination of cure depth [19]

3.2: Determination of Cure Depth

3.2.1 Photo-initiator (PI) Study

PI in the resin solution helps to initiate photopolymerization by generating radicals when photons excite it. The PI concentration in resin is varied to study its effect. For this study the PA and monomer concentrations of the resin solution are kept same. Thus, three different solutions were created each containing the same amount of monomer initial concentration, photo-absorber concentration (0.1%), oxygen concentration (21%) and different concentrations of PI: 1%, 2%, 3%. Following the sample preparation guide

as explained in section 2.2.3, the variation in cure depth at different exposure times and the bridge structures are measured.

Based on the measurements, the working curve is generated. From the figure 3.2, it is clear that cure depth increases as the PI concentration increases. Increasing photo-initiator concentration will generate more radicals when light is exposed. This will allow the radicals to react with more monomers that will eventually lead to a more curing and hence a larger cured depth.

From this figure however, it is not possible to determine the cut off conversion ratio. Conversion percentage of resin from liquid to solid will decrease as the depth of the resin in the vat increases as light cannot reach it. Thus, the conversion near the surface of the resin will be maximum. As depth increases, the resin will lose its ability to solidify and there will be a solid-liquid interface in the resin vat which is the cut-off percentage of conversion ratio that will be obtained by simulation analysis explained ahead.

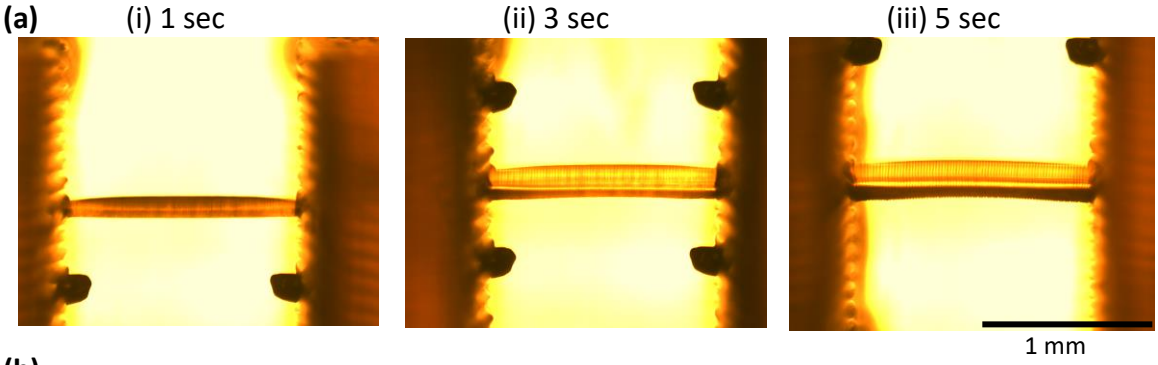

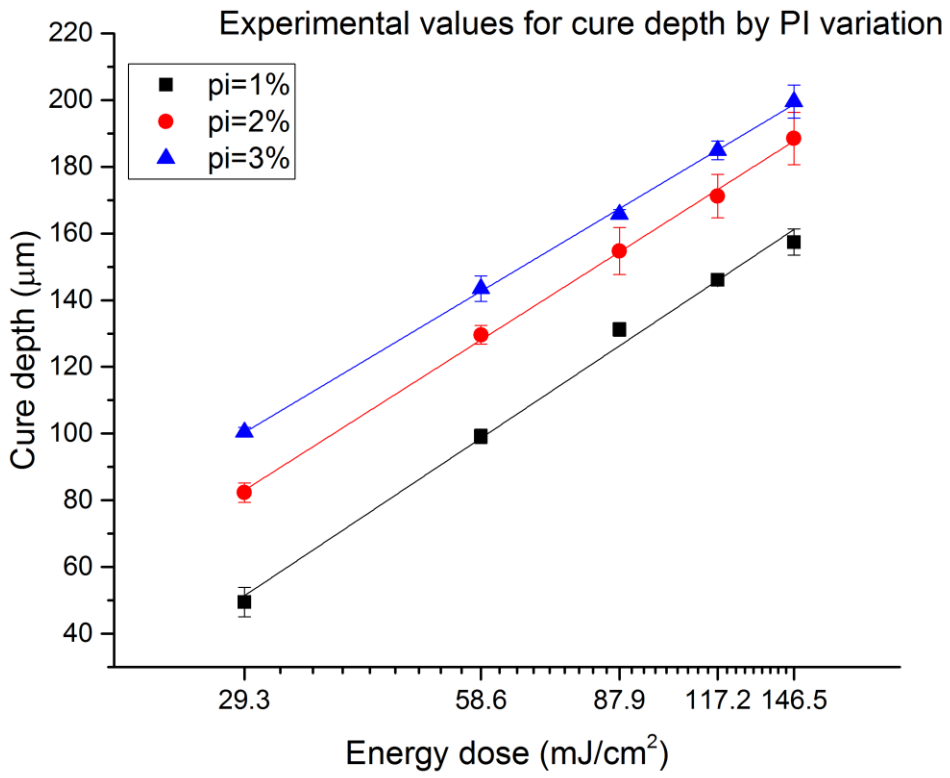

Figure 3.2 (a) (i, ii & iii) Represent bridge structures at [PI]=3%. The layer thickness of the bridges is measured and plotted for each varied [PI]. (b) Represents the experimental working curve where x axis is log scale energy dosage and Y axis is Cure depth. This graph shows increment in depth as [PI] in the system increases.

3.2.2 Photo-absorber [PA] Study

Photo-absorber is the other important constituent of the resin solution. It plays a vital role in 3D printing since it acts as a light absorber. It is therefore vital to see how the slope (D_p) and eventually C_d is affected by varying PA concentration. In this experiment, three solutions with [PA] of 0.05%,0.1% and 0.15% are prepared by keeping the [PI] at 2%, environmental oxygen concentration at 21% and monomer concentration constant. PA is usually added in very small quantities since larger amounts means that more light is absorbed rather than used for radical generation. It is generally observed from experiments that if the PA concentration is low, the structures are thicker. Therefore, if PA is absent, the structures will be thicker and sometimes partially cured. It should be noted that there is a large variation in layer thickness as the PA concentration increases. Working curves are plotted for each varied concentration of PA.

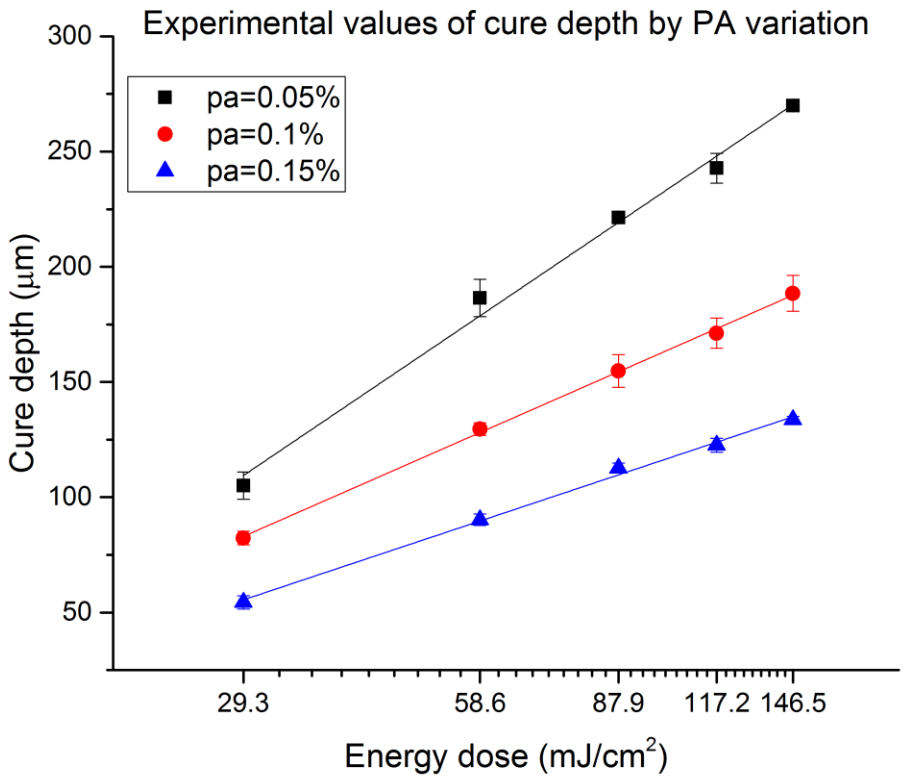

Figure 3.3 Working curve for experimental cure depth measurement by [PA] variation

3.2.3 Oxygen Inhibition Effect

Oxygen inhibition effect can be explained with the formation of a tacky layer on the surface. Environmental oxygen is continuously replenished on the surface of the resin. This creates a continuous supply of oxygen molecules (if the concentration is not controlled) to react with the radicals that are cleaved when light falls on PI molecules in resin. The stable peroxides do not contribute to reaction, however, due to high light intensity, the resin below the surface still polymerizes. The oxygen effect is noticeable because the top layer is not formed completely, and a gel like layer is formed above the

solidified layer. Due to this the overall structure may not form with the desired thickness and width.

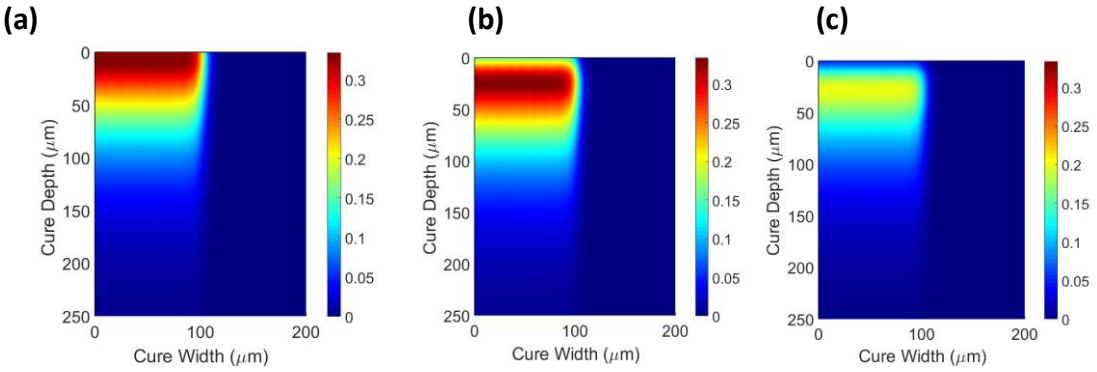

Figure 3.4 Effect of environmental oxygen on cure depth and conversion (a) Oxygen at 1% shows maximum conversion at surface and no tacky layer formation, (b) As oxygen concentration (10%) increases in the system, its effect on the surface is prominent, showing maximum conversion below the resin surface, (c) When oxygen is at atmospheric level (21%), the effect of inhibition layer is prominently seen by the blue region at the surface showing extremely low conversion percentage and formation of tacky layer.

The effect of oxygen on layer thickness can be established with the percent of atmospheric oxygen present in the surrounding and the height of the tacky layer formed because of its presence. Since the effect of PI and PA studies have validated the simulation in the section 3.3, this interesting effect of tacky layer formation can be expressed with the simulation domain. The Figure 3.4 explains how tacky layer increases as the oxygen concentration in the environment increases, thereby limiting the conversion on the surface.

3.2.4 Effect of Layer Thickness

Unlike PI, PA and oxygen concentrations, layer thickness is a structural control parameter. Every 3D printer has the ability to print a layer that has a known thickness.

When a CAD model of known dimension is converted into sliced images, the number of sliced images formed depend on the layer thickness inputted in the slicing software. Thus, if the layer thickness is small, there will be more sliced images that would lead to more print time. If the layer thickness is large, there will be less sliced images that will decrease the print time. The further analysis of layer thickness is done for surface roughness study in Chapter 4, where it plays a vital role.

3.2.5 Effect of Light Intensity

Energy dose variation is performed by increasing the exposure time of light on the resin surface. The intensity of light has a vital role in photopolymerization process. The intensity of light used in experiments is 29.3 mW/cm^2. Through simulation, the intensity of light is varied and its effect is studied on conversion ratio. The following Figure 3.5 shows effect of varying light intensity on cure depth. However, for the ease of experimentation, the light intensity is set to highest possible value, thus allowing it to be an initial condition value of setting up simulation.

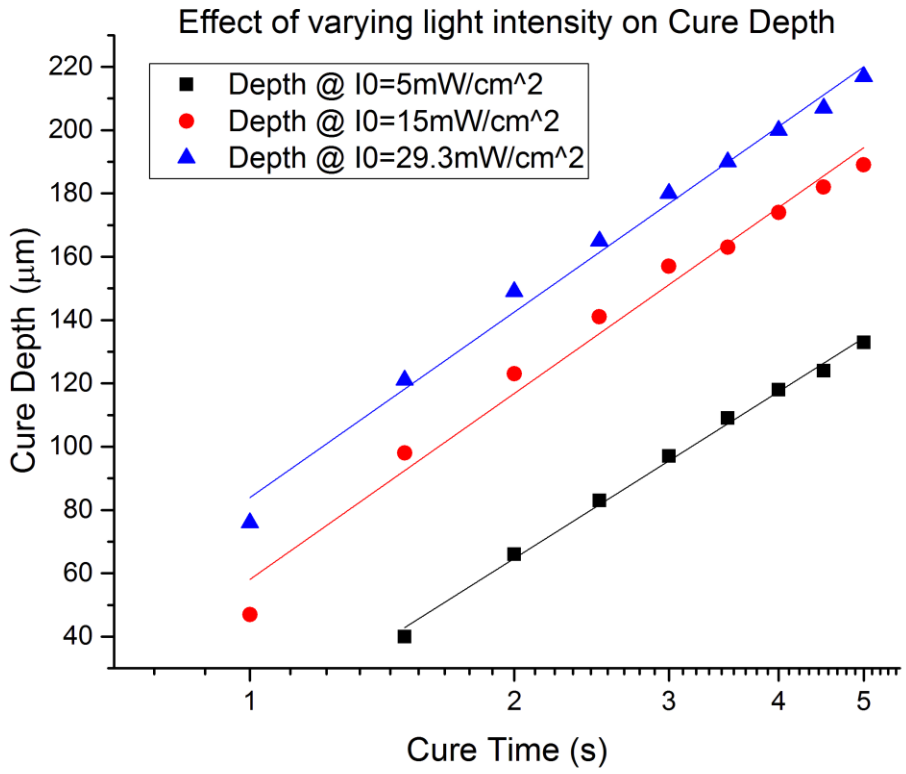

Figure 3.5 Effect of varying light intensity on Cure Depth.

This plot is obtained using simulation tool for the parameters of [PI]=2%, [PA]=0.1%, [O]=21%. The cure depth was measured at 4% conversion cut off. Increasing the light intensity will increase the energy dose that will result into increase of cure depth.

3.3 Model Validation: Experimental and Simulation Comparison

As discussed earlier, measuring the cure depth experimentally will not give the percentage of monomer that has converted into polymer. Revisiting equation 2.8, the conversion ratio *C* will depend on the initial monomer concentration ($[M]_0$) and the monomer concentration ($[M]$) remaining after the applied energy dose. The ratio is primarily important because *C* indicates the volume ratio of solidified part. The value of

C varies between 0 and 1. Zero indicates liquid resin while 1 indicates 100% conversion (solid polymer) [5]. Since the volume ratio is not directly estimated from experiments, the setup simulation will compute for the energy dose provided and will give *C* as output, which will be a percentage value. To obtain the conversion percentage, cure depth is estimated from the simulation at different conversion percentages or at different 'conversion cut-offs'.

As explained in section 3.2.1, conversion ratio cut-off will be selected at the interface of solid and liquid inside the resin vat. It is determined from the established computational model. The experimentally measured cure depth should abide to simulation curing depth. To obtain the simulation result, a time-progressing graph of conversion ratio and cure depth is established. On *y*-axis the conversion percentage is plotted while the *x*-axis represents the cured depth.

The progressive time curves are represented as a result. The *y*-intercept grid line intersects the time curve and the *x*-intercept at that intersection is projected on *x*-axis to find the cured depth. Different *y*-intercept values are selected, meaning different conversion percentages are selected and the cure depths are measured for different times. Figure 3.6a shows the time-progressive graph while figure 3.6b shows cure depths at different conversion ratios.

To validate the model, iterative analysis is performed on simulation values of 'k_o', 'α', 'α_a', '$[O]_0$' and '*C*'. These values are selected because these constants in the simulation affect the cure depth and the slope. The iterative values are chosen based on research guidelines from [5] to [20] and the range of acceptable values are picked until the

iterative result gives agreeable D_p and C_d simulation and experimental value. The table 4 explores how sensitive curing depth result is to the selected parameters.

Table 4 Fitting Parameters

Parameter		Effect on **slope (D_p)** when parameter increases	Effect on **cure depth (C_d)** when parameter increases	Fitting parameter Value	Literature value range	Source
Symbol	Name					
k_o	Oxygen inhibition constant	Decreases	Decreases	15 $m^3/mol/s$	10 – 5 x 10^5 $m^3/mol/s$	[9] & [8]
α	PI molar absorptivity	Decreases	Increases	11.9 m^2/mol	4.6 – 20 m^2/mol	[20] & [5]
α_a	PA molar absorptivity	Decreases	Decreases	4600 m^2/mol	4600 m^2/mol	[5]
$[O]_0$	Initial oxygen concentration	Remains same	Decreases	0.9 mol/m^3	~1 mol/m^3	[8]
C	Conversion ratio cut off	Remains same	Decreases	Measured %	-	-

The values of the fitting parameters are reported at varied range in literature as shown in table 4. For validating the model, the effect of these parameters on the cure depth (C_d) and slope (D_p) is studied. First, a random set of fitting parameter values are selected to obtain conversion ratio cut-offs (*C*) at different percentages. Based on the effect of varying conversion ratio cut off on D_p and C_d, a value is selected allowing to study the next parameter: molar absorptivity of PA (α_a). By selecting a literature value, its effect on D_p and C_d is studied by performing simulations. During this time α, k_o, $[O]_0$ and *C* kept constant. An iterative analysis is thereby performed on each parameter while keeping the remaining values fixed. The final simulation obtained D_p and C_d should be close or equal to experimentally observed values.

(a)

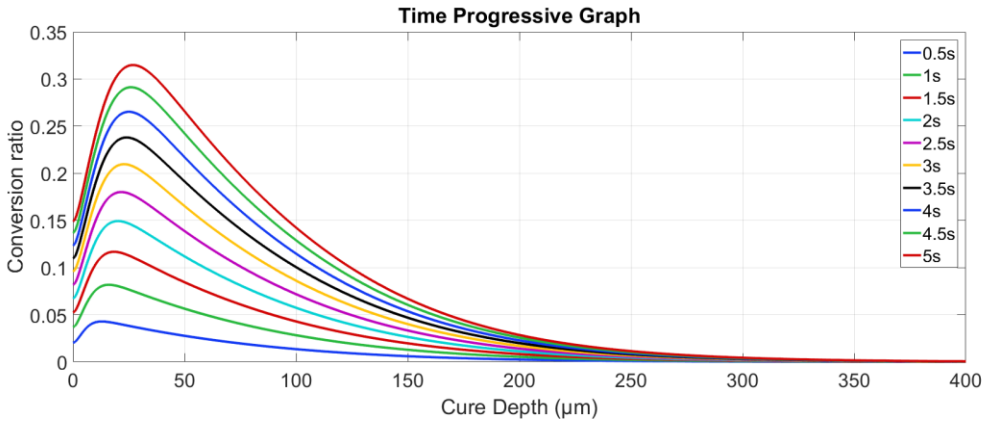

(b)

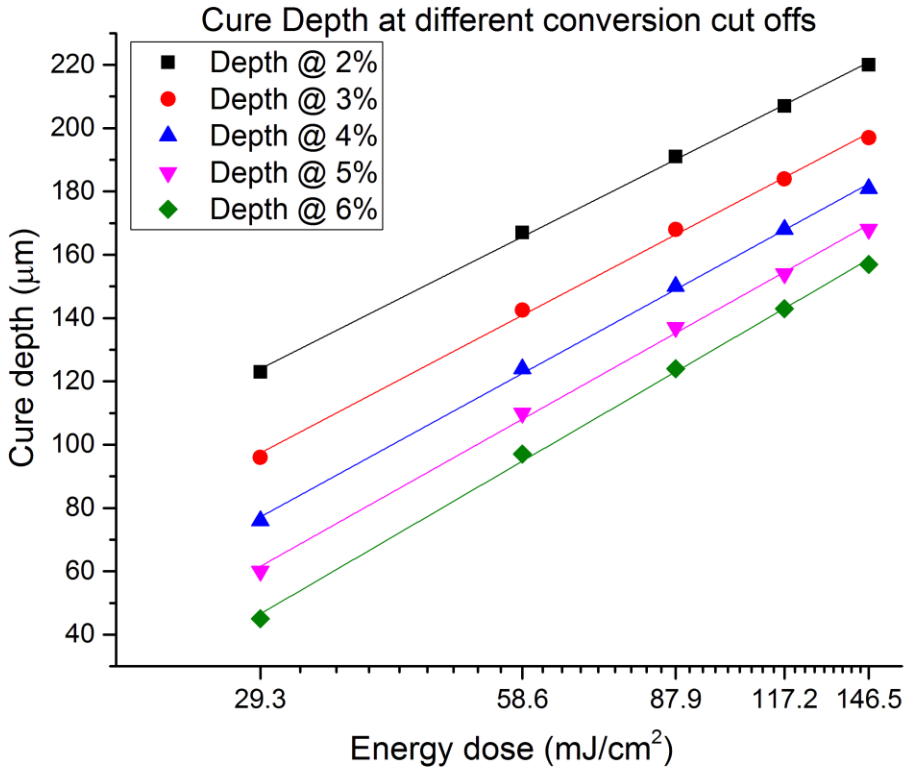

Figure 3.6 (a) Time progressive graph plots conversion ratio vs cure depth, giving cure depth from different conversion ratios (b) Working curve for Cure depth vs Energy dose for different conversion ratio cut offs. The cut off will be selected based on the slope and depth that closely matches with experiment.

From the iteration results of fitting parameters, simulation obtained cure depth at 4% conversion cut off agrees well with experimental data. This selected conversion ratio cut off is set to be final for all the experiments performed. To validate the model, the cure depths obtained from simulations and experiments are checked for different solutions. A working curve showing the simulation and experimental agreement is shown in Figure 3.7. The slope, which represents D_p and the cure depths C_d are matched for validation analysis, which is shown in the table below.

Table 5 D_p comparison for experiment and simulation for [PI] effect on depth at 4% conversion cut off

[PI] %	Experimental D_p (µm)	Simulation D_p (µm)
1%	140.6 ± 2.2	152.9 ± 2.8
2%	149.7 ± 2.9	150.1 ± 1.5
3%	140.2 ± 2.4	148.3 ± 2.1

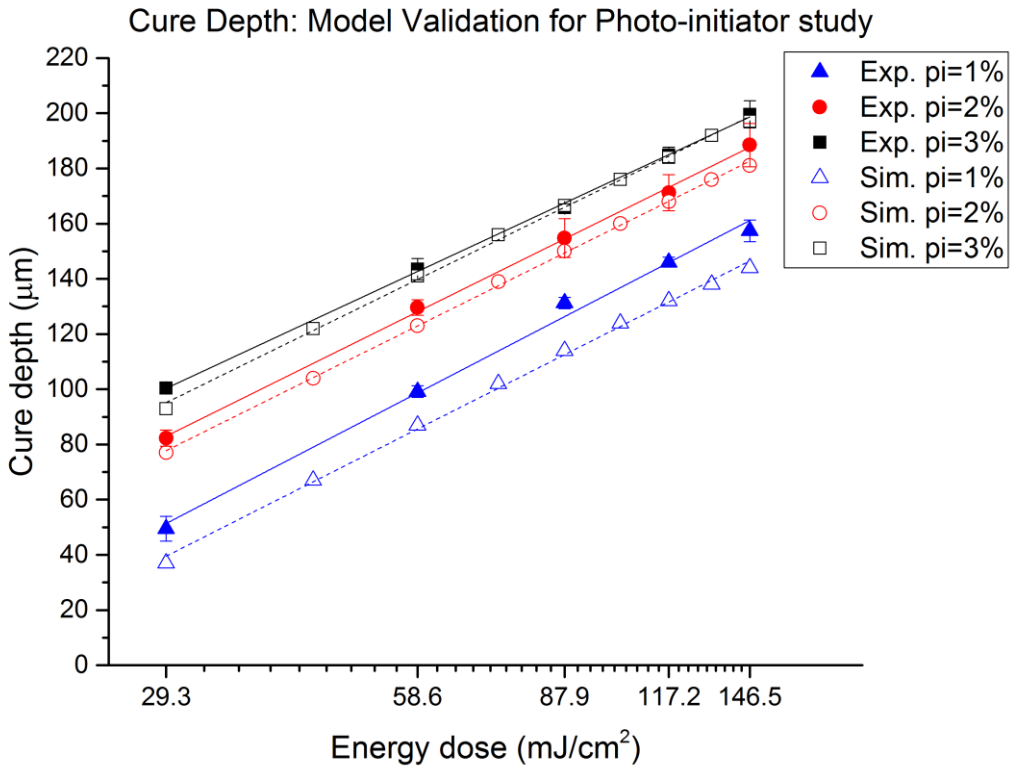

Figure 3.7 Cure Depth: Model Validation for Photo-initiator study

As the conversion cut off is already established in PI study, the same percent of cut off is used to find the cure depth using simulation. It is seen that the simulation agrees well with PA concentration of 0.1% and 0.15%, but it is highly sensitive to at 0.05%. It is seen from experiments as well that the cure depth is sensitive at 0.05% but the simulation over-estimates the values at that particular PA concentration. However, it is also seen that there is a good agreement with the slopes of the empirical working curves and the simulation working curves. This means that the simulation will predict over-estimated cure depth value for PA concentration of 0.05% at the selected cut-off, however will be able to give accurate result for slope, i.e., the penetration depth, which is the characteristic value to be determined.

Figure 3.8 shows the agreement between the experimental and simulation results at the cut off of 4%. Now that the simulation is validated for cure depth study using PI and PA, we can establish confidence in the simulation and use it for evaluating the effects of all the parameters on cure depth and cure width.

Table 6 D_p comparison for experiment and simulation for [PA] effect on depth at 4% conversion cut off

[PA] %	Experimental D_p (μm)	Simulation D_p (μm)
0.05%	230.2 ± 11	255.1 ± 5.8
0.1%	149.7 ± 2.9	150.1 ± 1.5
0.15%	113.6 ± 3.9	99.6 ± 1.6

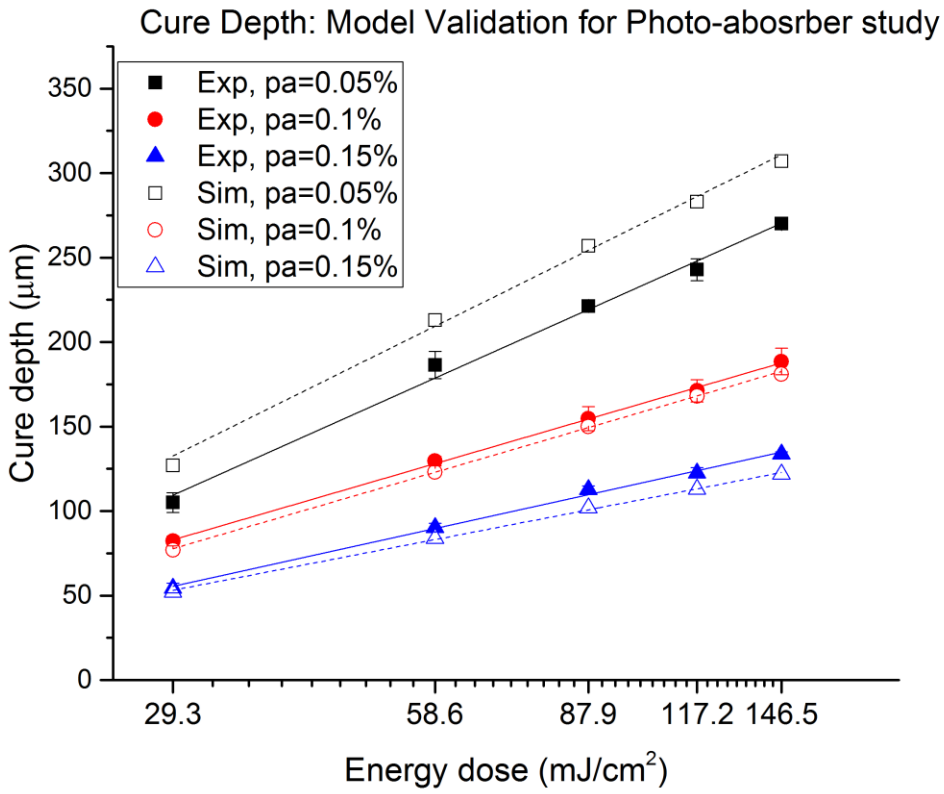

Figure 3.8 Cure Depth: Model Validation for Photo-absorber study

3.4 Evaluation of Printing Parameters

3.4.1 Effect on Curing Depth

Since the parameters to select are abundant and each variation has critical effect on the printing quality, i.e., the cure depth and width, evaluation of each parameter is necessary. For optimal quality 3D printed parts instead of viewing parametric variation in multiple graphs, a single graph is constructed to study the impact. The following table will show what parameters are varied.

Table 7 Printing parameter evaluation using normalized value concept

Parameter	Normalized Parameter				
	A: 0.5	**B: 1**	**C: 1.5**	**D: 2**	**E: 2.5**
[PI] %	1%	2%	3%	4%	5%
[PA]%	0.05%	0.1%	0.15%	0.2%	0.25%
I_0 (mW/cm^2)	10	20	30	40	50
[O] %	5%	10%	15%	20%	21%
Time (s)	1sec	2sec	3sec	4sec	5sec

The column B was used first to determine the curing depth and width at those parameters that fall under the value. A singular value of cure depth is obtained for this set of parameters for the previously selected cut off ratio of 4%. After singular value generation, simulations were computed for each possible combination and results for parameter for that normalized value was obtained. For example, if effect of PI is to be studied, the value of PI at column A, B, C, D & E are used and the values of remaining parameters are selected from column B. Then when PA effect is to be studied, values of PA are varied but the remaining parameters have their values fixed. This method provides simulation data that will allow to study the effects of each parameter on cure depth.

From the figure 3.9, it can be inferred that when [PI] increases, the curing depth will increase. When [PA] concentration increases, the cure depth decreases. When environmental [O] increases, the tacky layer height increases but overall depth remains same. When light intensity increases, the cure depth increases, and at last when exposure time increases, the cure depth also increases. This guideline establishes that most of the parameters increase the cure depth.

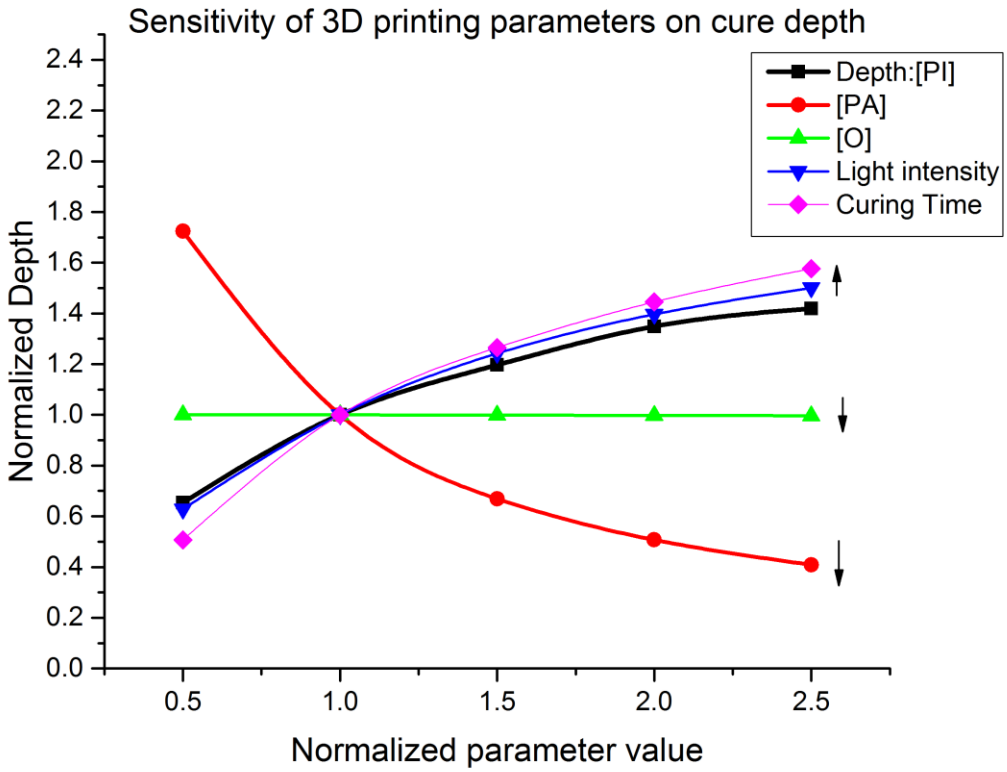

Figure 3.9 Effect of printing parameters on cure depth

This result implies how sensitive to variation cure depth values are when printing parameters are changed. It can be observed that [PA] will primarily affect the depth, which can also be validated through figure 3.8 and table 6, where D_p and C_d both decrease as [PA] increases. The least effective is environmental oxygen concentration which, as explained before contributes to tacky layer formation.

This analysis, however falls short of providing the optimal print process parameters. Also, cure depth does not give complete idea about the layer profile. Since layer profile will be the fundamental in determining print process parameters for high-quality

structures, it is therefore important to address the effect of varying parameters on cure width as well.

3.4.2 Effect on Curing Width

Each layer formed will be at the surface of the resin and the parameters that affect the depth will not have a similar effect on the width of the 3D structure. Cure width of a 3D printed part is not elaborately evaluated in previous research, but the result is important to determine the surface quality as changes in width (either thicker or thinner) will not only affect the print but may make or break the print. Therefore, it is necessary to observe the cure width as well.

Experimentally, the cure width is dependent on the width of the beam. The projection of the sliced image on the surface of resin will have a beam width that has diameter (in microns) equal to the number of pixels that are in the image. When the light passes through the reduction lens, its resolution is reduced, thus each pixel will have a conversion factor in microns. For the PμSL system, the conversion is 12 microns/pixel. Thus, depending on the dimension of the CAD model, the beam width in pixels will be projected, which when printed should have dimension as designed in the CAD system. Studying the effect of curing width also allows to determine the minimum environmental oxygen concentration that can fairly print fine structures. Fig 3.10 shows that when oxygen concentration is kept to 0%, the printed structures are wider and completely ruin the critical parts of print, by over-curing during each layer. As oxygen concentration is increased in the system and the print is repeated, at 5% [O], the print is acceptable and structurally reliable.

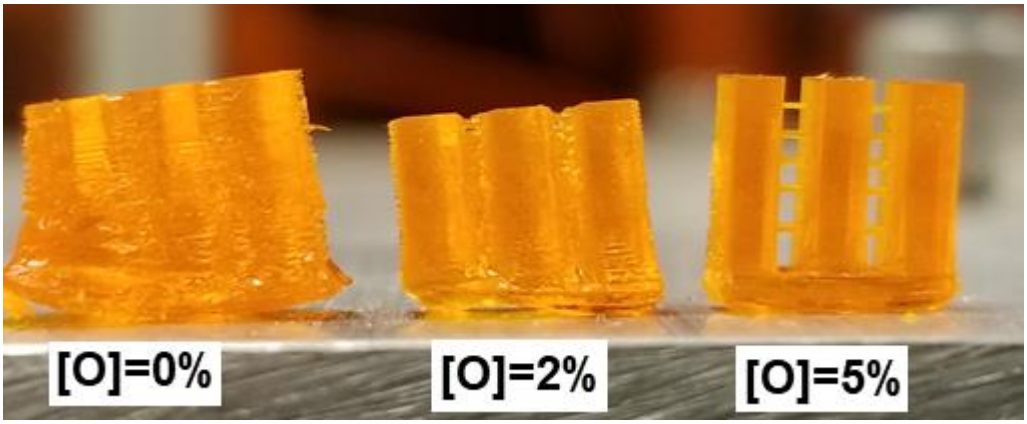

Figure 3.10 Effect on oxygen concentration on 3D Printing. It is concluded through experimentation that printable structures indeed require a minimum of 5% oxygen in the surrounding to fabricate the structures.

A similar simulation is repeated for the finding the variation of cure width by varying the parameters. Referring to Table 7, the values were extracted from the simulation to give following result.

From figure 3.10, it can be inferred that oxygen concentration has the highest effect on curing width and that as oxygen concentration increases, the cure width decreases, which was to be expected after the result discussed above. It is also comprehensible that as [PI], light intensity and exposure time increase, curing width increases. The cure width increases with increase in most of printing parameters.

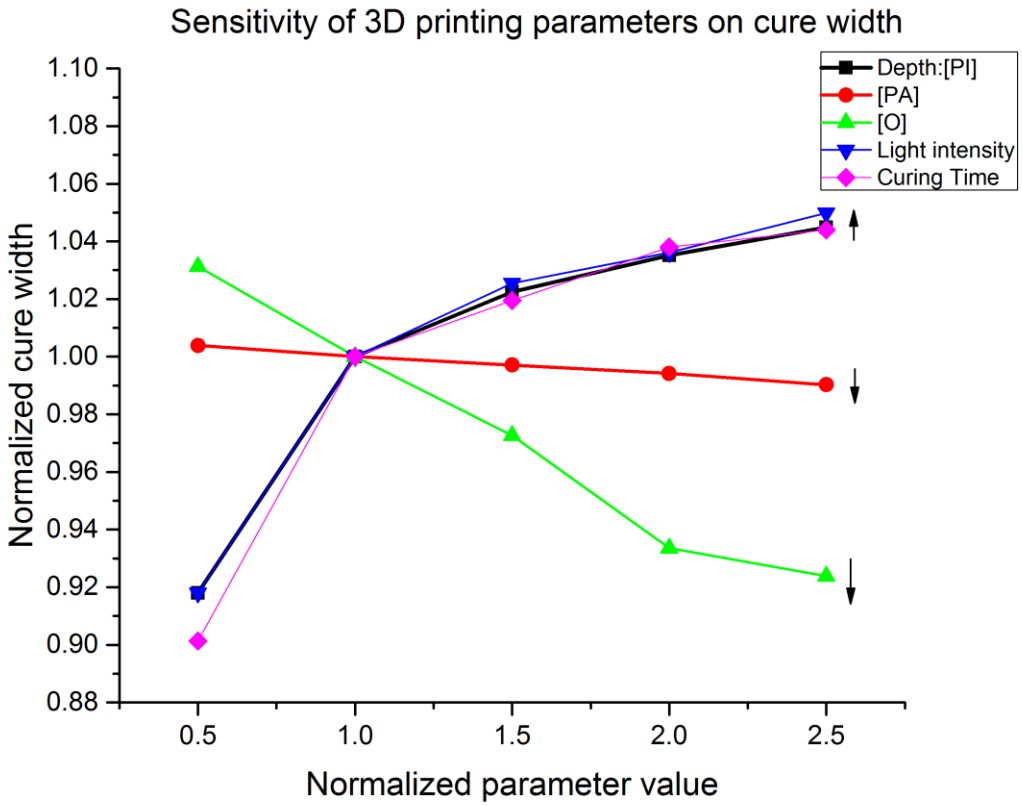

Figure 3.11 Effect of printing parameters on cure width

3.5 Effect of Varying Parameters on Conversion Ratio and Layer Profile

As the effect of varying printing parameters on cure depth and cure width is established, the simulation tool can be used to understand the important role the resin species play while photopolymerization takes place. Since, the parameters are varied according to Table 1, their effect on the photopolymerization process can be studied by observing conversion ratio and the layer profile.

3.5.1 Effect of Varying [PI] on Conversion Ratio and Layer Profile

Each printing parameter will affect the resin species as photopolymerization progresses. When [PI] is varied, it impacts the generation of radicals, propagation of monomers and

also changes the percent of conversion and layer profile. As [PI] increases, the radical generation increases, thereby attacking larger number of active monomers which directly results in more conversion. This can be shown by the simulation result below. The parameter for [PA] is 0.1%, [O] is 21% and overall conversion is observed.

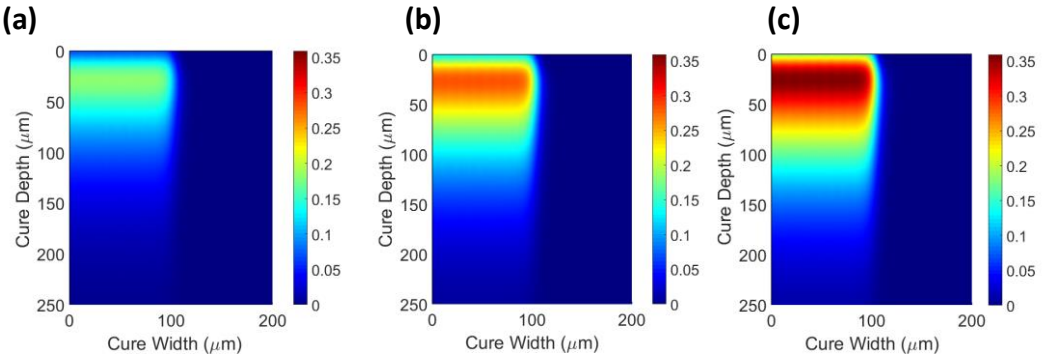

Figure 3.12 Effect on conversion ratio and layer profile by varying Photo-initiator concentration. (a) Overall conversion when [PI]=1% Minimum conversion takes place giving minimum cure depth at 4% conversion cut off (b) Conversion and cure depth increases as PI concentration is increased to 2% (c) Maximum conversion and cure depth when PI concentration is maximum (3%)

3.5.2 Effect of Varying [PA] on Conversion Ratio and Layer Profile

Similar analysis is done by varying the photo-absorber concentration in the simulation. The parameters for [PI] and [O] are fixed at 2% and 21%. The result shows that as [PA] increases, the absorber species dominate the reaction when UV light is irradiated by absorbing light. This results in lesser radical generation and eventually lower monomer propagation that results in lower cure depth, lower conversion and if the [PA] is not controlled, photopolymerization may not take place. The effect on conversion ratio and layer profile can be observed by the simulation result below.

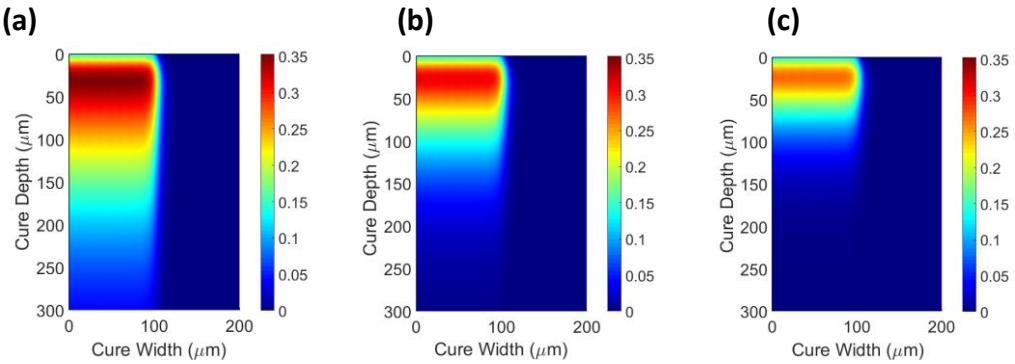

Figure 3.13 Effect on conversion ratio and layer profile by varying Photo-absorber concentration. (a) Overall conversion when [PA]=0.05% Maximum conversion takes place giving maximum cure depth at 4% conversion cut off (b) Conversion and cure depth reduces as PA concentration is increased to 0.1% (c) Minimum conversion and cure depth when PA concentration is maximum (0.15%)

3.6 Summary

The computational model is validated by matching the slope of working curves for the experimentally observed values and simulation data. This foundation allows to progress to the next stage of the research, i.e., the prediction of surface profile of 3D Printed parts.

4 Estimation of Surface Roughness of 3D Printed Parts

In this chapter, the confirmation of the validation allows to proceed further with the analysis of surface roughness. The 2D domain that represents the resin in the vat can further be utilized to show the surface profile of the cured layer. It will guide to establish an observation to see the side profile change by variation of the parameters. At the same time, the surface roughness value is extracted from the 3D structure by image processing. An effective way to define surface roughness is by calculating the root mean square (RMS) value. Taguchi Analysis is used to find optimal print process parameters with the help of RMS value.

4.1 Layer Profile Study

4.1.1 Layer Profile Analysis Using COMSOL

The conversion ratio contour plot is studied to identify the shape of the layer that is polymerized. The shape considers the cure width and the cure depth. Due to the Beer-Lambert law, the light attenuation inside the resin will form a trapezoidal shape as it cures. The cured layer at the surface will be wider, while the bottom of cured layer will smaller. This shape of the layer is noticeable as the conversion ratio cut off is varied. The bridge structures provide a cure depth that does not have a preset layer thickness. But while 3D printing structures, layer thickness is an input condition. Each layer is formed based on the layer thickness value. To observe this via simulation, the layer profile with complete cure depth is extracted from 4% conversion cut off and the extracted profile is limited to the input layer thickness provided for 3D printing. Thus, conversion cut off will determine the shape of the layer.

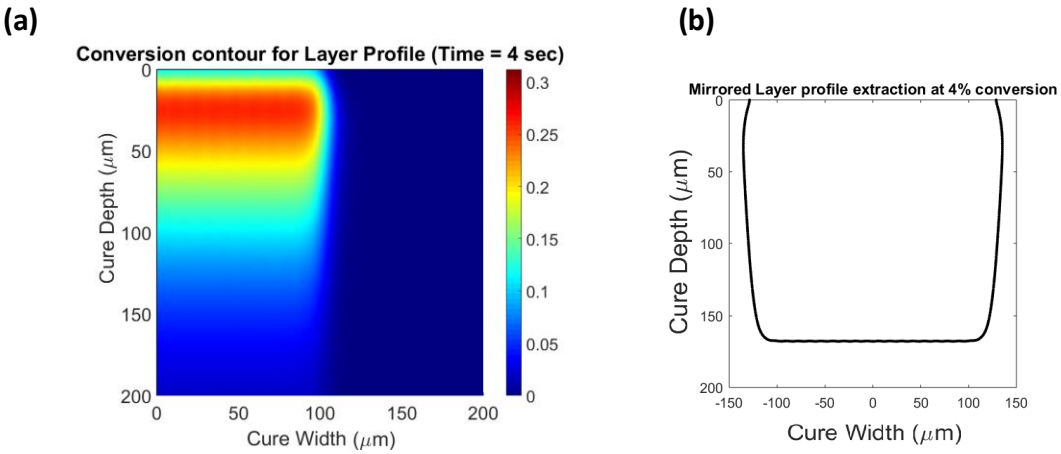

Figure 4.1 Conversion contour layer profile extraction. (a) shows simulation data, (b) The data is extracted at 4% to form a shape of the cured profile.

Figure 4.1(a) shows the 2D domain conversion plot and 4.1(b) shows the mirrored layer profile at 4% conversion. The layer profile data is extracted from COMSOL and the extracted data is exported to MATLAB. The exported data is the entire layer profile and is the natural cure depth that represents the solid-liquid resin interface at 4% conversion. For the data extraction purpose, layer profile is critical than the layer thickness, because layer thickness can later be manually implemented to match with the experimental layer thickness that is provided to a 3D printer's stage. Thus, in 3D printing, the stage on which layers are printed will lower with a preset distance, which is the layer thickness of each layer.

4.1.2 2D Representation of a 3D Strut by Layer Stacking

The purpose of extracting the layer profile is to utilize it to form a shape of a strut that represents 3D printed layers. Due to the conversion characteristics, the trapezoidal shape will be common to all the layers, thereby forming the stair-stepping effect. Taking

inspiration from the additive nature of manufacturing, additive approach is used to stack extracted layer profile on one other.

The selected layer profile with preset layer thickness will be stacked on one another to represent a 3D printed strut that is completely generated using MATLAB. Programming the 3D strut into a 2D stacked layer format builds the foundation for estimating the optimal print process parameters.

Thus, the layer-by layer process can be assumed to highly repetitive in producing same layer profiles if 3D printer is set correctly. Therefore, the assumption that each layer profile will be similar allows to duplicate the layer formed in simulation to be stacked one below the other, where the top layer will represent the newest layer formed and the lower layer will be the earlier printed layer. Figure 4.2 elaborates the 3D strut 2D stacked layer representation.

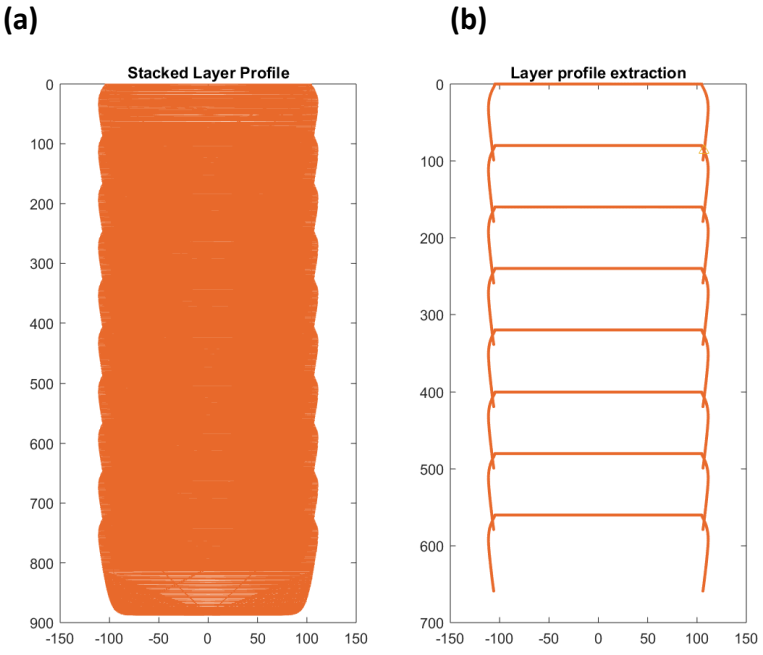

Figure 4.2 2D Strut: (a) 3D printed strut representation. (b) Layer profile stacking

4.2 Surface Roughness

Surface roughness is represented either by R_a, which is arithmetic average height of roughness-component irregularities from the mean line, measured within the sampling length or by RMS (R_q) which is the root mean square or the geometric average height of roughness-component irregularities within the sampling length. In this study, RMS is selected as a roughness measure because it amplifies occasional high and low readings, meaning it takes into consideration the entirety of roughness irregularities while R_a just considers average heights.

4.2.1 Surface Roughness (RMS) Measurement of Strut Using Image Analysis

ImageJ software is used to detect edges and further process the image so that it can be used to obtain RMS value. Firstly, the printed part is kept under a 5x magnification lens and an RGB surface profile image is taken by focusing on the edges of the struts. The light is illuminated from below to remove the shadow effect of layers on top of each other. The picture is saved with a resolution of 1024x1280 pixels. The image is then loaded with the ImageJ software and the edges are selected by selection tool. The option 'Find Edges' is selected, which highlights the edges in the selected region. These detected edges are shown in Figure 4.3a. The next step is to extract these edges. A tool in image processing called 'Find Maxima' is used to extract the edges. The profile of the detected edges is shown in Fig. 4.3b. This tool extracts the edges based on the noise tolerance. If noise tolerance is too tight, the extracted edge will not be resolved enough to show the complete side profile, but as the tolerance is relaxed, a very articulate profile can be extracted.

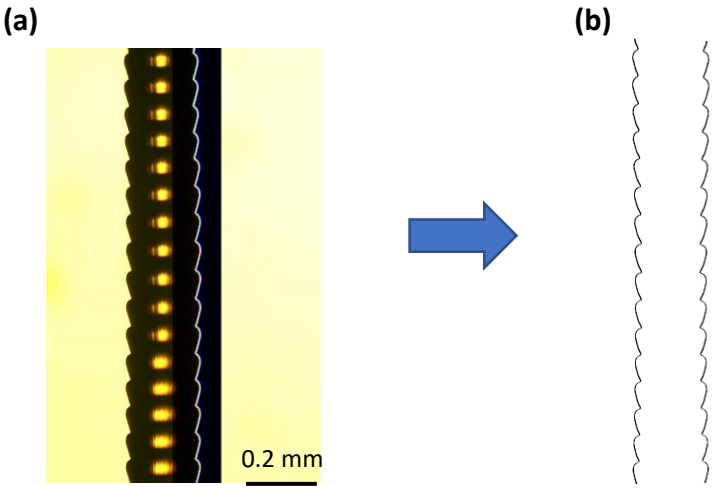

Figure 4.3 (a) Edge detection using ImageJ **(b)** Edge extraction using ImageJ

However, it is not possible to obtain a strut that is exactly vertical. Due to placement of the structure on the microscope and the ability of the camera to rotate, a tilt error can cause the image to slightly incline. This tilt angle will cause experimental measurement error while determining the surface roughness. To address this issue, the tilted image is adjusted by rotating to an optimal 90° position, which can be performed in ImageJ by using the straightening option. The straightening tool adjusts the user-selected pixels in the image to align them, thus reducing the tilt. This creates a perfectly vertical layer profile to estimate RMS.

According to ASME B46.1, RMS is the root mean square average of the profile height deviations from the mean line, recorded within the evaluation length [21]. The formula to calculate RMS is given by,

$$RMS=\sqrt{\frac{(\sum_{i=1}^{n} Z^2)}{n}} \qquad (4.1)$$

In equation 4.1, Z is the magnitude of profile deviations from the mean line and n is the total number of profile deviations. Mean line is drawn on the detected edge, by choosing pixel index that is the average between the maximum peak and minimum tip of the edge profile. The magnitude of each profile deviation is determined by the pixel distance between the mean line and the edge profile. The important part is the sampling length. To further maintain the tilt of the edge profile, eight layers are chosen at random (eight corresponding layers that have minimum tilt) over which the RMS formula is applied. Using equation 4.1, the surface roughness value is determined in pixels, which is converted into microns. Figure 4.4 shows the implementation of the ImageJ tilt correction and RMS formula to determine the surface roughness. The coding to determine surface roughness is done in MATLAB.

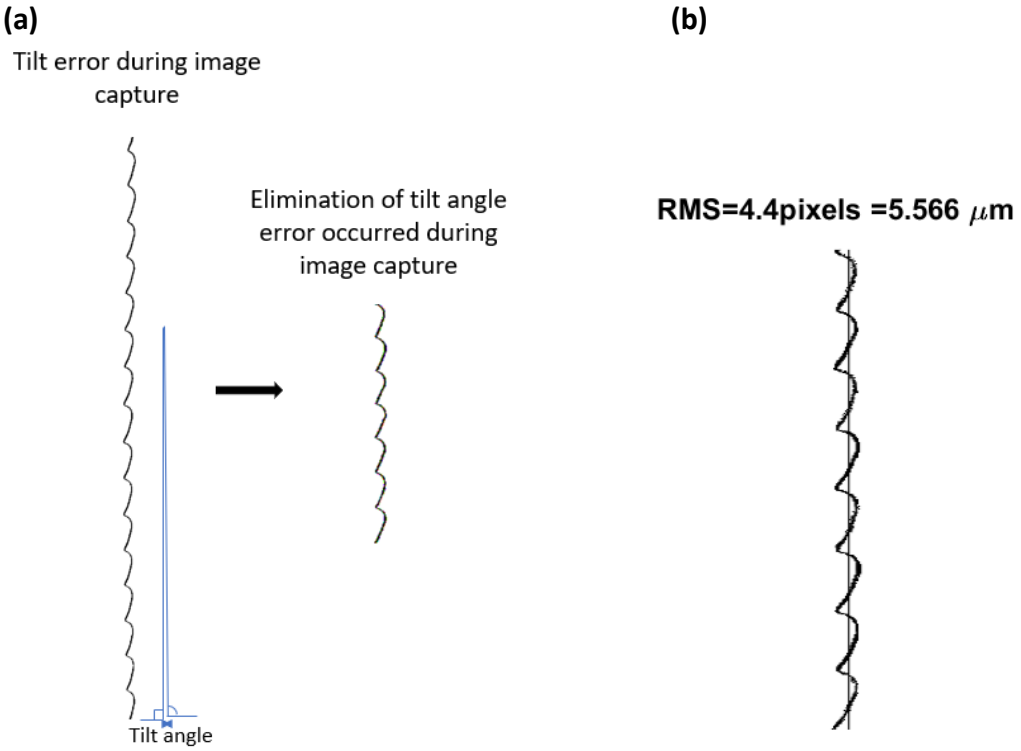

Figure 4.4 (a)Edge profile tilt error elimination (b) Experimental RMS calculation

4.2.2 Surface Roughness (RMS) Measurement from 2D Represented Stacked Layers

As developed earlier, the 2D representation of stacked layers is used to determine the RMS value through simulation. The stacking of top layer on the lower layer, as shown in Figure 4.2, creates a point of intersection. These points of intersection between two layers are dependent on the layer thickness that is preset to form the stacked strut visualization. The lower region of the top layer will intersect on the surface of the lower layer, which forms the side profile.

Since the sampling length in experimentation is for eight layers, the MATLAB generated strut is also formed for eight layers to maintain valid comparison. To calculate profile deviations from simulation, the data selected is first filtered to remove a part of the layer profile. The data in consideration, which is solely the edge profile, is stored separately in an array in MATLAB.

The next step is to plot mean line over the selected edge profile to measure the profile deviations. A similar approach is utilized to find the mean line. The peak and lowest tip of the surface related irregularities is found out from the edge profile. The mean of all the values in between the peak and tip is calculated, which is plotted on the edge profile that represents the mean line.

Now that the sampling length and mean line is determined, the next part is the find the magnitude of the profile deviations from the mean line. Using Euclidean distance formula, the magnitude of profile deviations for each point on the edge profile is calculated. Using the RMS formula, the surface roughness is determined. The code is

developed in MATLAB. Figure 4.5(a) shows the edge profile selected and 4.5(b) shows the mean line and the surface roughness RMS value.

(a) **(b)**

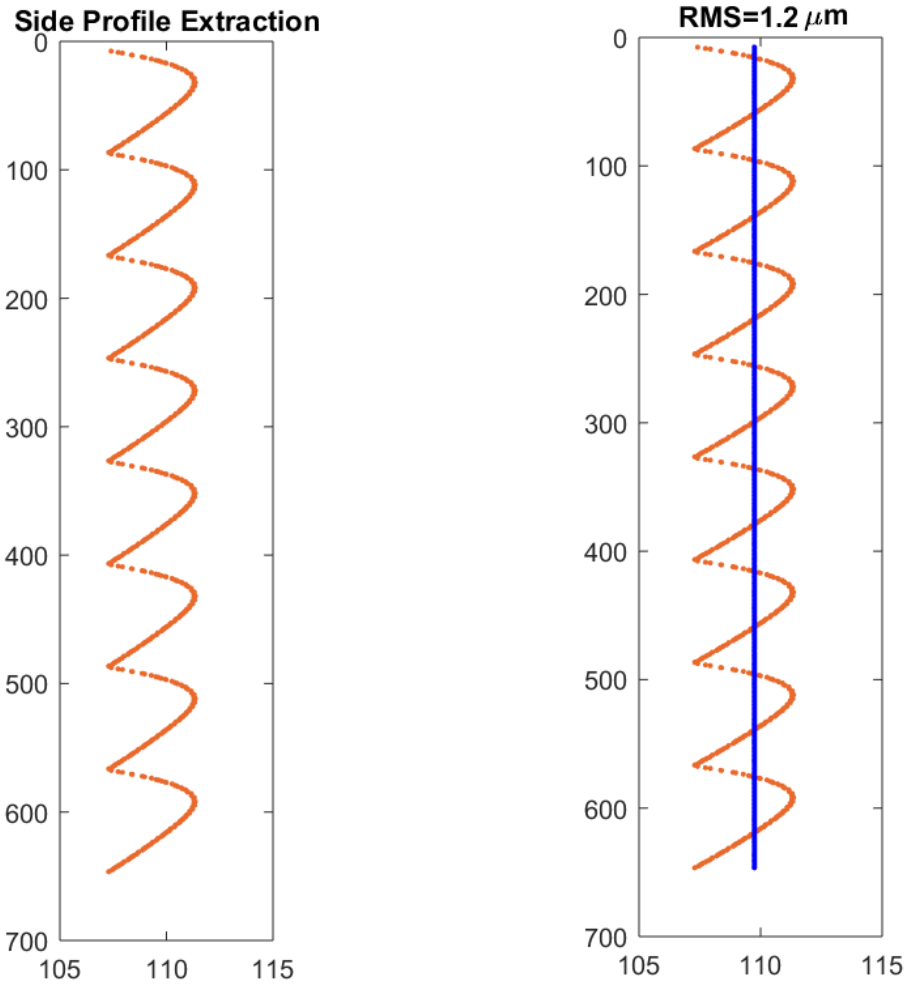

Figure 4.5 (a) Side profile extracted from simulation data (b) RMS from simulation

4.3 Parameter Study

4.3.1 Taguchi Orthogonal Array

4.3.1.1 Introduction to Probabilistic Design of Experiments

For 3D printing experiments, the goal is creating high quality 3D printed parts. Next is to determine the requirements to achieve this goal. This step in any design of experiment (DOE) is crucial because if the requirements are classified incorrectly, the function parameters that need to studied to fulfill the requirement will differ, thereby resulting into error of goal achievement. For the purpose of our study, the requirement is to have minimal surface roughness to achieve the defined goal.

The next step is to study the functional parameters that fulfills the requirement. The functional parameters will have varied levels, and to select what level of each functional parameter will give optimal result, a probabilistic DOE is required. In general, experimenting by varying the factors and level is time-consuming and costly.

Taguchi invented the concept of robust design that would drastically reduce the number of experiments to be performed. His method is known as the Taguchi Method of Orthogonal Arrays. Figure 4.6 shows the steps involved in DOE for this study.

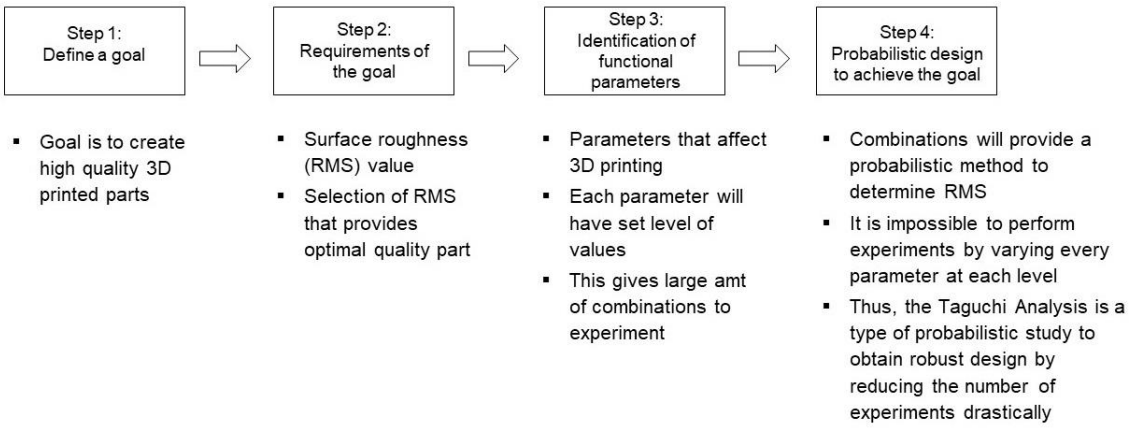

Figure 4.6 Steps for developing a robust DOE

4.3.1.2 Importance of Taguchi Method

Taguchi method is used to reduce the number of experiments to find optimal parameters that will give the robust result of the experiment. It states that the design of the part produced must exactly adhere to the target value. If the part deviates from the target value, there is loss. Larger the deviation, larger is the loss. The number of experiments to be performed depend on number of factors and number of levels. Each parameter that affects the goal is called a factor. Each factor will have set of values, which are known as levels. Based on the number of factors and levels, an orthogonal array (OA) is generated which suggests the number of experiments to be performed. Each experiment will have factors at different level. Taguchi recommends to perform the experiments as organized in the orthogonal array and the output of each experiment is the goal that is required to be found. Taguchi developed standard arrays based on number of factors and their levels. Taguchi's OA is represented as follows:

$$L_N(S^K) \tag{4.2}$$

Where *N* is number of experiments to be performed, *S* is the number of levels of each factor and *K* is the number of factors.

4.3.1.3 Implementation of Taguchi Method

Based on evaluation of parameters, the factors selected are [PI], [PA], [O] (environmental oxygen concentration), Layer thickness (LT) and curing time (CT). There are three levels for each factor, thus the total number of possible combinations obtainable for optimal result are 3^5. To reduce the number of experiments, Taguchi OA of $L_{27}(3^5)$ is selected from the standard tables available. To validate whether the selection is correct, the degree of freedoms is calculated. The DOFs should be less than the number of experiments. The DOF is given by,

$$\text{DOF}=1+ (\text{No. of factors}*(\text{No. of levels} - 1)) \quad (4.3)$$

For this study, the DOF is 11 and from the list, the only available Taguchi Array is $L_{27}(3^{13})$. The factors and their levels are shown in table 8.

Table 8 Factor and levels for Taguchi OA

Levels	Factors				
	[PI] %	[PA] %	[O]%	Layer thickness (µm)	Curing time (s)
1	1	0.05	10	100	2
2	2	0.1	15	80	3
3	3	0.15	21	50	4

4.3.2 Validity of Surface roughness

From Figures 4.4 and 4.5, it is evident that the experimental surface roughness and simulation surface roughness is different for same parameters. To check the validity of surface roughness through simulation, random experiments from the Taguchi's OA are performed to check if the trend is followed. The reason for difference between

experimental and simulation RMS is the fact that the simulation underestimates the variation in cure width. The table below shows the Taguchi OA along with RMS as response. Each experiment number's factor levels were input in the simulation along with their RMS result. Further analysis is performed in next section.

Table 9 Taguchi orthogonal array with RMS as response

Experiment No.	PI	PA	O	LT	CT	RMS
1	1	0.05	10	100	2	**1.6**
2	1	0.05	10	100	3	**1.2**
3	1	0.05	10	100	4	**1.1**
4	1	0.1	15	80	2	**2.9**
5	1	0.1	15	80	3	**1.8**
6	1	0.1	15	80	4	**1.6**
7	1	0.15	21	50	2	**2.5**
8	1	0.15	21	50	3	**1.5**
9	1	0.15	21	50	4	**1.2**
10	2	0.05	15	50	2	**0.5**
11	2	0.05	15	50	3	**0.4**
12	2	0.05	15	50	4	**1**
13	2	0.1	21	100	2	**2.7**
14	2	0.1	21	100	3	**2.1**
15	2	0.1	21	100	4	**1.7**
16	2	0.15	10	80	2	**4.5**
17	2	0.15	10	80	3	**2.7**
18	2	0.15	10	80	4	**2.2**
19	3	0.05	21	80	2	**0.8**
20	3	0.05	21	80	3	**0.7**
21	3	0.05	21	80	4	**0.7**
22	3	0.1	10	50	2	**0.7**
23	3	0.1	10	50	3	**0.6**
24	3	0.1	10	50	4	**0.6**
25	3	0.15	15	100	2	**5**
26	3	0.15	15	100	3	**3.6**
27	3	0.15	15	100	4	**3**

If the experimental surface roughness is low, the simulation result also shows smaller roughness value. Thus, it can be said that the simulation surface roughness will offer a

guideline to select optimal factor level combination, and that the lowest obtained simulation roughness value will eventually lead to optimal quality 3D printed part. This validity can be checked in Case Study 1.

4.3.3 Optimal Factor Level Selection Using Sensitivity Analysis

Once the RMS is obtained for every experiment in OA, sensitivity analysis is performed to find the optimal levels for each factor.

4.3.3.1 Sensitivity Analysis

To find optimal factor levels, signal to noise ratios are found for each experiment. The signal to noise or SN ratios measure how the response (RMS value) varies relative to target value (the expectation set to find optimal factor levels). The factors that are controllable are called signal values, which are the parameters listed in table 8. The noise factors are not controllable, but can be controlled during experimentation, which is the response, i.e., RMS of the analysis.

As the signal and noise factors are identified, SN ratio is determined. Depending on the goal of the experiment, there are three different SN ratio measures,

a) Larger the better
b) Smaller the better
c) Nominal is the best

The SN ratio option is chosen by the goal requirement. Since minimum surface roughness will give high quality 3D printed parts, '*smaller the better*' is chosen to evaluate the factor levels. The formula to calculate SN ratio for smaller the better is given by,

$$\text{SN ratio} = -10 * \log_{10}\left(\frac{\sum Y^2}{n}\right) \quad (4.4)$$

In equation 4.4, Y means responses of given factor level combination, i.e. RMS for this case and n is the number of responses in given factor level combination, i.e., n=1. Using the formula, table 10 records RMS response and SN ratio for each experiment.

The calculations are done on Minitab software, which allows to perform sensitivity analysis.

Table 10 SN ratio analysis for Taguchi OA

Experiment No.	PI	PA	O	LT	CT	RMS	SNRA1
1	1	0.05	10	100	2	1.6	**-4.0824**
2	1	0.05	10	100	3	1.2	**-1.58362**
3	1	0.05	10	100	4	1.1	**-0.82785**
4	1	0.1	15	80	2	2.9	**-9.24796**
5	1	0.1	15	80	3	1.8	**-5.10545**
6	1	0.1	15	80	4	1.6	**-4.0824**
7	1	0.15	21	50	2	2.5	**-7.9588**
8	1	0.15	21	50	3	1.5	**-3.52183**
9	1	0.15	21	50	4	1.2	**-1.58362**
10	2	0.05	15	50	2	0.5	**6.0206**
11	2	0.05	15	50	3	0.4	**7.9588**
12	2	0.05	15	50	4	1	**0**
13	2	0.1	21	100	2	2.7	**-8.62728**
14	2	0.1	21	100	3	2.1	**-6.44439**
15	2	0.1	21	100	4	1.7	**-4.60898**
16	2	0.15	10	80	2	4.5	**-13.0643**
17	2	0.15	10	80	3	2.7	**-8.62728**
18	2	0.15	10	80	4	2.2	**-6.84845**
19	3	0.05	21	80	2	0.8	**1.9382**
20	3	0.05	21	80	3	0.7	**3.098039**
21	3	0.05	21	80	4	0.7	**3.098039**
22	3	0.1	10	50	2	0.7	**3.098039**
23	3	0.1	10	50	3	0.6	**4.436975**
24	3	0.1	10	50	4	0.6	**4.436975**
25	3	0.15	15	100	2	5	**-13.9794**
26	3	0.15	15	100	3	3.6	**-11.1261**
27	3	0.15	15	100	4	3	**-9.54243**

The negative values in the SN ratio column in table 10 are analogous to the signal theory, since the use of SN ratio formula from equation 4.4. For any type of goal (from (a), (b) or (c)) to be achieved, the highest SN ratio will correspond to the factor levels that will give robust result. Since the expression has negative sign, the SN ratios which will give a result closest to 0 or more than 0 will be the optimal factor levels or the experiment numbers that should be selected to achieve high-quality 3D printed structures.

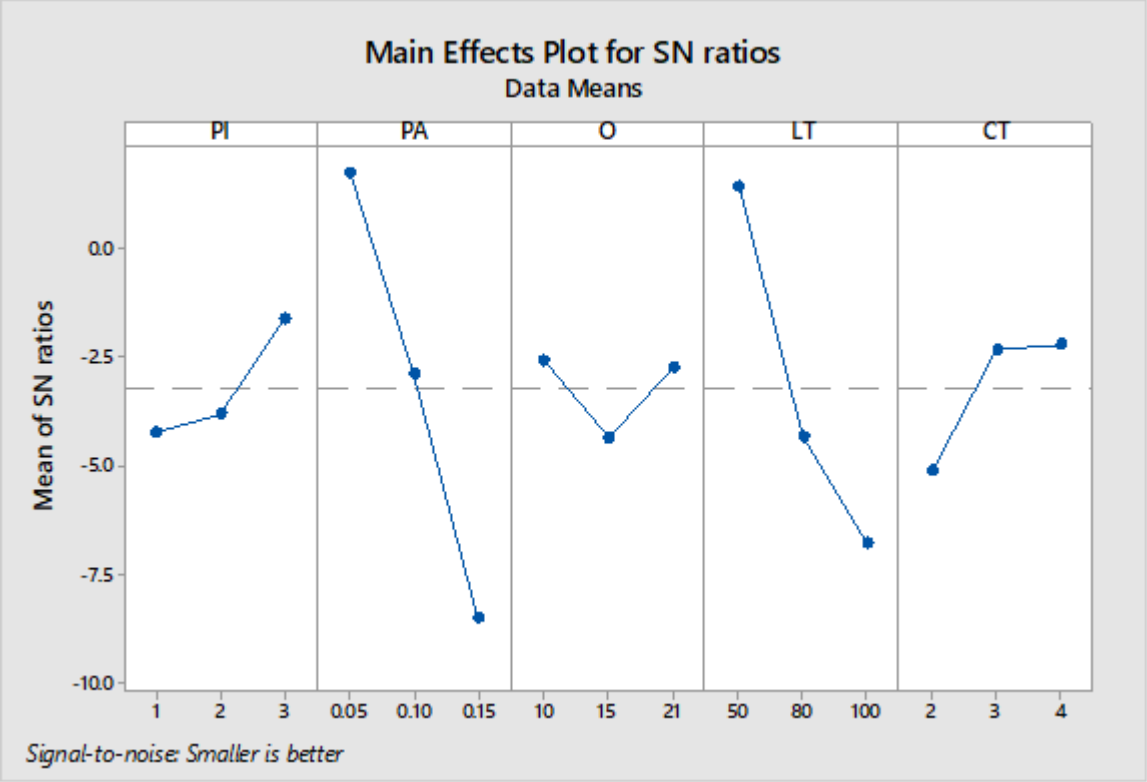

Figure 4.7 SN ratio analysis based on RMS response of Taguchi Experiments. The level corresponding to the maximum value of mean of SN ratios is selected for each factor.

Table 11 Response Table for Signal to Noise Ratios: Smaller the better

Level	PI	PA	O	LT	CT
1	-4.222	1.736	-2.562	1.432	-5.1
2	-3.805	-2.905	-4.345	-4.316	-2.324
3	-1.616	-8.424	-2.735	-6.758	-2.218
Delta	2.606	10.208	1.782	8.190	2.883
Rank	4	1	5	3	2

Main effects plots for SN ratios are generated. The plots can be read to give two important results. First, it helps to identify the optimal level to choose for getting the goal and secondly, it determines which factor has the maximum effect on the response. Figure 4.7 shows the Main Effects plot.

Along with the plot, a response table (table 11) is generated that delivers delta and rank of values. It identifies the factors that have the largest effect on the response. The response table calculates the average value of each level for each factor. For e.g., the factor Curing time had 3 levels: 2 secs, 3 secs and 4 secs. In the OA, level of 2 seconds appears 9 times. That means there are 9 SN ratios that have level of 2 seconds. The average of that 9 values is calculated. This procedure is repeated for each level of every factor to generate the response table data and establish the rank.

In figure 4.7, Y axis represents the SN ratios and X axis represents factor levels. The average SN ratio of the response is represented by the dotted line. The average SN ratio of each level for each factor is plotted and a line joins the dots. The goal is to maximize the SN ratio irrespective of the type of analysis. Thus, the maximum SN level ratio point on graph for each factor will be the optimal factor to achieve the minimum surface roughness, i.e., the response.

Thus, from figure 4.7, the optimal factor levels selected are,

a) [PI]= 3%

b) [PA]= 0.05%

c) [O]= 10%

d) Layer thickness= 50 um

e) Curing time= 4 secs

The rank represents which factor affects response the most. Rank is based on the delta value, which is the difference between the highest and the lowest average SN ratio value of levels for each factor. From the response table, the primary effect on surface roughness is due to PA concentration and the least effect is due to oxygen concentration.

4.3.3.2 Experimental Validation

To validate the Taguchi Analysis, a final experiment is performed with the optimized factor levels and the simulation and experimental surface roughness is compared by considering the following case studies.

4.4 Case study 1: Roughness for Straight Strut Using Optimized Factor Levels

By using optimized factor levels, experiment was performed to 3D print struts and do analysis on their surface roughness. The validated result ensures that the printed part using these parameters will have high-quality. The printed strut and the validated surface roughness are shown below. Since oxygen concentration shows the least effect, it was kept at 21%

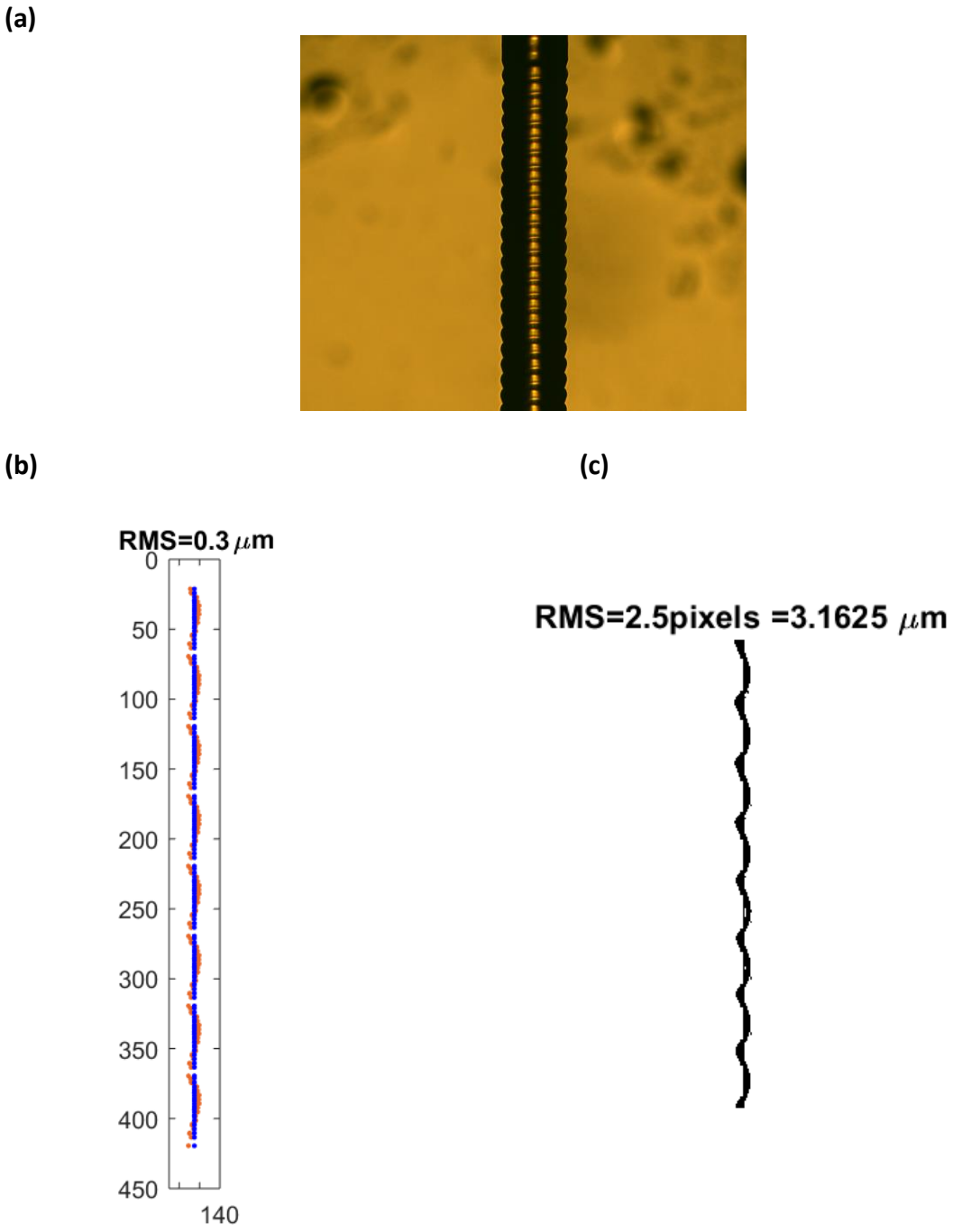

Figure 4.8 (a) 3D High-quality strut printed using robust printing parameters from Taguchi Analysis, (b) Simulation obtained RMS shows lowest roughness for high-quality strut & (c) Experimentally obtained surface roughness is compared with (b) that verifies lowest achievable RMS by varying printing parameters.

To validate the hypothesis, nominal parameters are chosen. With [PI]= 2%, [PA]=0.1%, [O]=21%, Layer thickness= 80 microns and curing time of 5 seconds, a strut is printed and compared between experimental RMS and simulation-based RMS with optimized and improved high-quality strut shown in Figure 4.8. It can be seen that the surface topography of the vertical strut with optimized parameters, when compared with strut with nominal parameters, is improved by approximately 40%.

(a)

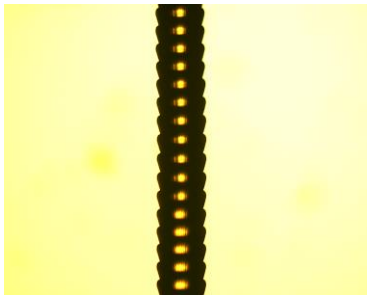

(b) **(c)**

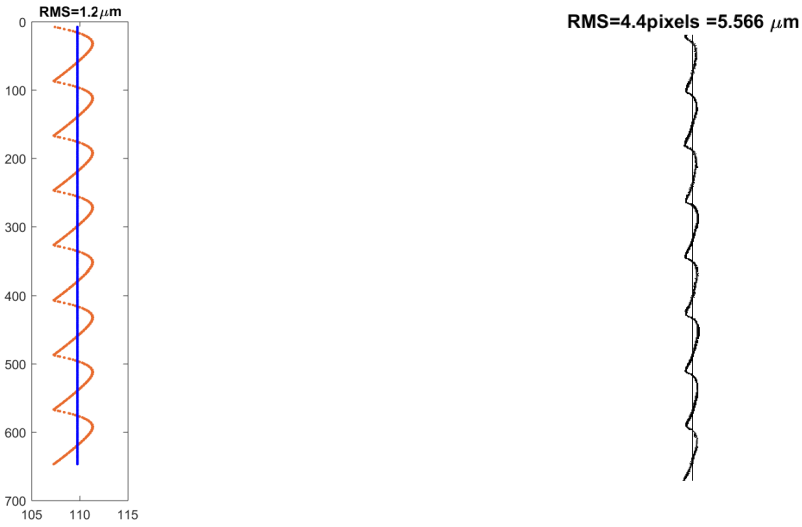

Figure 4.9 Nominal factor comparison. (a) Strut printed with unoptimized parameters leading to higher roughness, (b) Simulation-based RMS shows higher roughness, (c) Experimentally obtained value shows higher roughness, thus indicating Taguchi analysis will help minimize surface roughness and provide high-quality structures by pre-processing printing parameters.

However, using optimized values faces a limitation. Time required to print the structure with optimized layer thickness, irrespective of other parameters, will be more. Time required to print a structure is given by,

$$Time_{total} = Time_{layer} * \text{Number of layers} \quad (4.5)$$

In equation 4.5, $Time_{total}$ is the total printing time and the number of layers depend on the bitmap sliced images generated by the slicing software when a layer thickness is applied to the CAD model. $Time_{layer}$ is time required to print one layer, given by

$$Time_{layer} = Time_{exposure} + Time_{stage} + Time_{wait} \quad (4.6)$$

In equation 4.6, $Time_{exposure}$ is the time the UV light is exposed on resin surface, $Time_{stage}$ is the stage time required by the linear stage sample holder to lower for next layer to form (measured to be 5s) and $Time_{wait}$ is the time allowed for the resin to refresh and the cured layer to adhere to its shape before the next layer can be formed. Exposure time and wait time can be modified depending on the requirement. Generally, they are kept same of each layer. Since concentrations of resin solution do not have a major impact on print time, the layer thickness study is done against total print time using following parameters: 2% PI, 0.1% PA and 21% environmental oxygen. This set of parameters were chosen because in model validation, this set appears to be common for PI and PA study on cure depth and width, as discussed in sections 3.2.1 and 3.2.2. Figure 4.10 explains the tradeoff of printing time and quality of 3D printed structure.

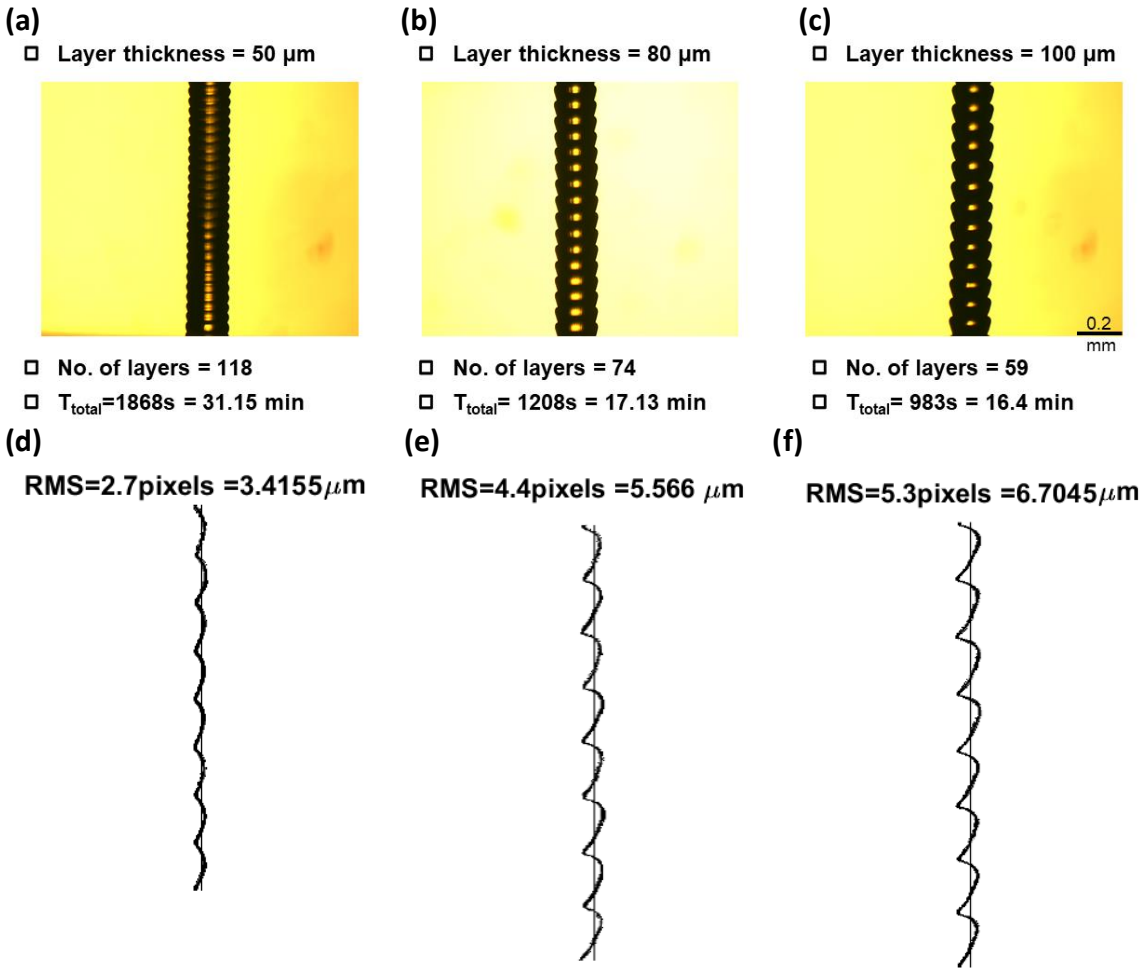

Figure 4.10 Time quality trade off. (a), (b) and (c) show the change in number of layers and time required to print as layer thickness is increased, also showing degradation in quality. (d), (e) and (f) show their respective experimentally obtained surface roughness values.

Based on the above analysis, optimized level structure is still preferable because even if it takes longer to print a singular structure, it has already saved trial and error experimentation time to achieve those levels.

To validate the hypothesis, the simulation is also run for the set parameters and the respective generated RMS is shown below. This confirms that performing a simulation can help in obtaining lowest possible surface roughness and allow printing for a high-

quality 3D printed part. The observed trend suggests that as the layer thickness increases, the difference between the simulation-based RMS and experiment-based RMS decreases. Comparison between Figure 4.10 (d), (e), and (f) and Figure 4.11 (a), (b), and (c) shows that when layer thickness is 50 µm, the difference between simulation and experimental RMS is almost 6 times while, as the layer thickness increases, for 100 µm, the difference is almost 4 times. It can be therefore be suggested that the with change of printing parameters, the trend either increases or decreases. The difference between the experimental RMS and simulation RMS can be studied on case to case basis.

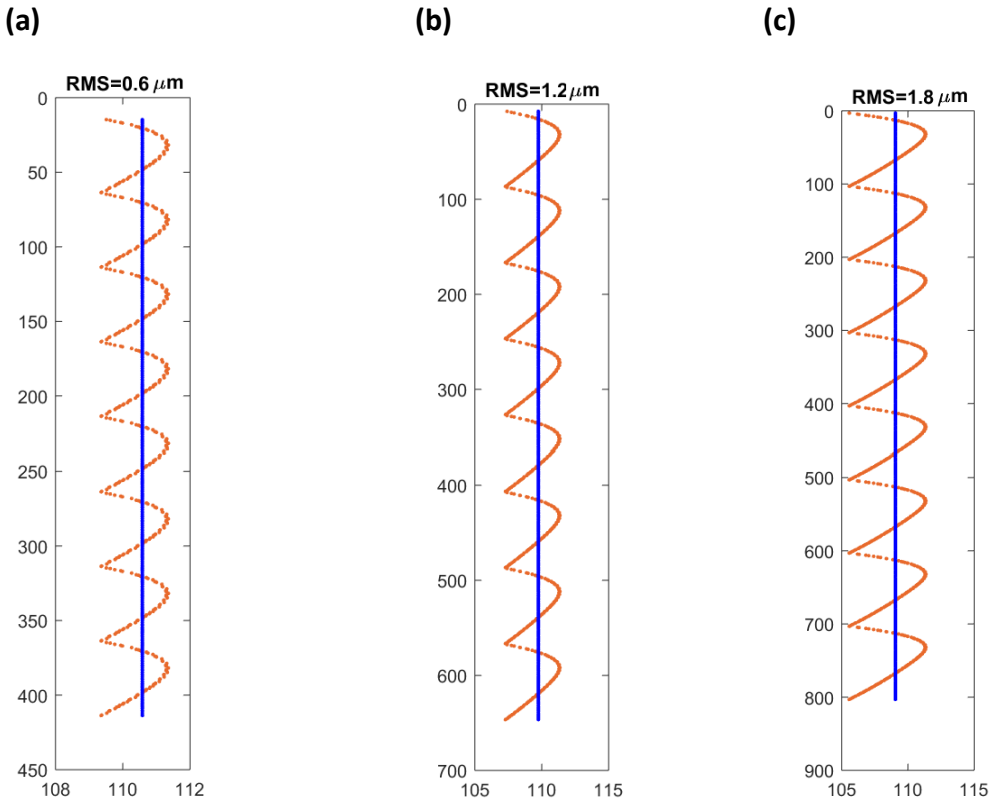

Figure 4.11 Simulation RMS values following the trend from experimental analysis. Roughness increases as layer thickness increases (a)RMS with layer thickness= 50 µm, (b) RMS with layer thickness=80 µm & (c) RMS with layer thickness= 100 µm

Above analysis assumes that photo-initiator, photo-absorber and oxygen concentration does not affect printing time however, they will affect the surface roughness. To save printing time when large number of samples are to be printed, the OA can be utilized. The OA will guide to achieve high quality structures without investing into increasing number of layers by simply choosing right fit of parameters. The SN ratio analysis will guide to eliminate the factor levels that will give extremely rough structures (SN ratios having least values). Therefore, if layer thickness is sacrificed to save time, following variations in accordance to OA and SN ratio analysis will still ensure close to high-quality structures:

Using mid (2%) to high (3%) level of [PI], low (0.05%) to mid-level (0.1%) of [PA]. Using around 15% environmental [O] and using 4 to 5 seconds of curing time. This will not only save time while producing large batches of structures, but also ensure that a high quality is maintained throughout the fabrication process.

The effect of layer thickness due to unoptimized set of parameters will be prominently seen in overhung structures, such as the bridge structure. The effect can be reduced by setting the layer thickness of the overhung structures to a Taguchi recommended depth, thus maintaining the quality of the overall structure.

4.5 Case study 2: RMS Roughness for Angled Struts Using Optimized Factor Levels

3D printing is fascinating because it is able to print complex structures. Printing a vertical strut is relatively easy. However, many of the CAD geometries such as micro lattices and honeycomb structures, rely on inclined structures for their highlighted features. Such inclined structures are considered in this study.

The uniqueness of this study is based on the inclination angle. Depending on the angle, the shape of the strut will be formed. When an inclination angle is included, the next layer printed is shifted by a particular distance. Therefore, the sides of strut will show different roughness. A smoother and sharper surface is observed in a single structure. Since the top layer is shifted by a particular distance, it will cure more than the preset layer thickness and overlap the layer below it on the side opposite to inclination angle. The overlapping will result in smoother surface, while the side parallel to inclination line will show a sharper surface. This can be shown in figure 4.12.

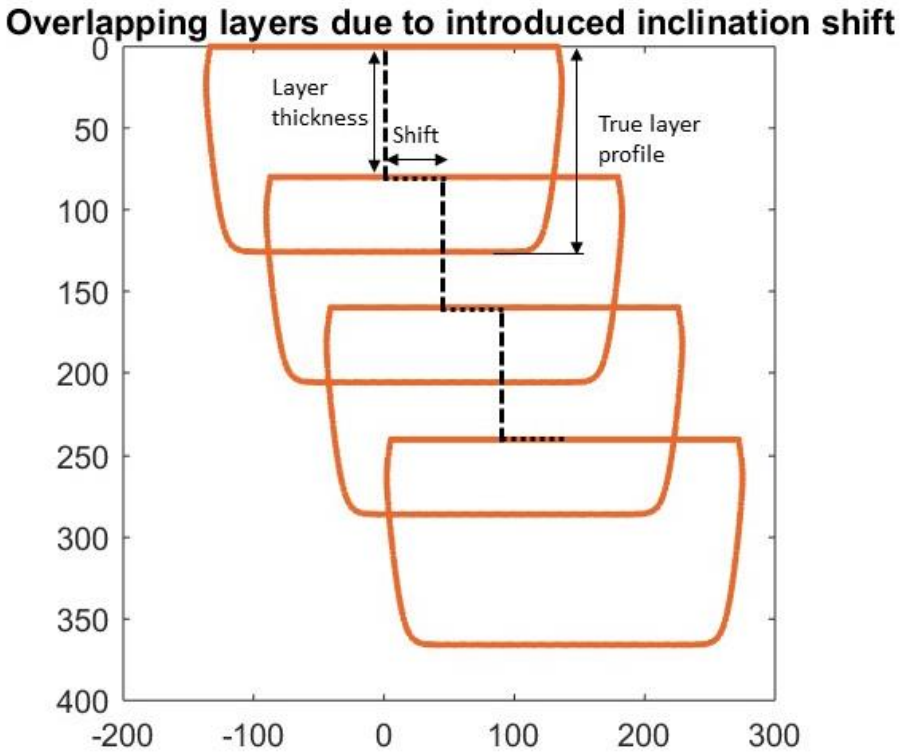

Figure 4.12 Top layer overlapping the layer below it due to shift distance.

The side profile of the inclined strut will be different on left hand side and right-hand side of the strut, thus having different surface roughness on each side.

The stacked layer 2D structure will be modelled based on the inclination angle given and the optimized factor levels. The inclination angles studied are 30°, 45° and 60° . These angles are chosen because based on the triangle properties, the sides opposite to these angles will represent the shift distance required to model the 2D stacked structure.

Consider the right angled triangle analogy shown in figure 4.13.

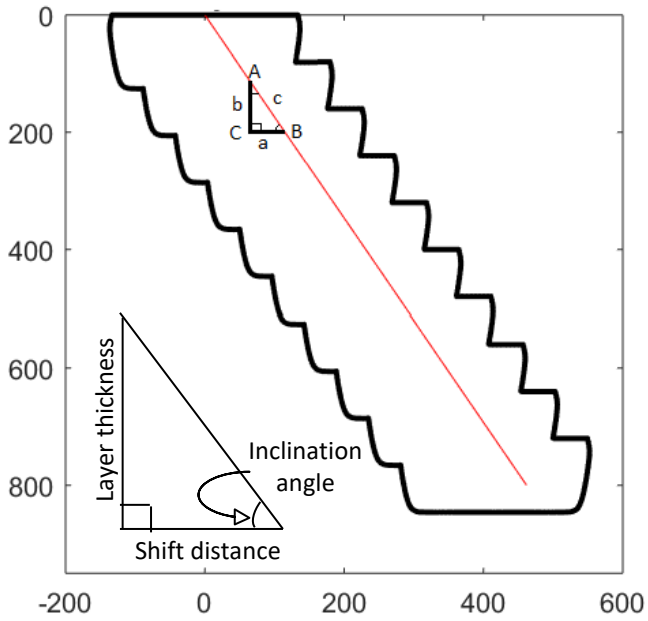

Figure 4.13 Right angled Triangle analogy for inclined strut

The length 'b' (µm) is the layer thickness. Since the light falls on resin surface, each layer will be printed in 90°, however, since the next layer will be shifted because of the inclination angle, the light will fall at a different location on the surface, by taking into consideration the shift. The layer thickness is the measure of side opposite to that of inclination angle, the side opposite to 90° will be the hypotenuse and the shift distance will be the side opposite to remaining angle. Thus, the shift distance for 30° inclined struct is given by the length of side opposite to 60°. Once the shift is determined, it is used in MATLAB to model an angled struct using the optimized factor levels.

Both edges of the angled strut will have different surface roughness due to overlapping effect which can be optimized based on the surface which is critical to quality. Since there are two edges, three cases are studied.

First, left edge is selected critical to quality, meaning that minimum surface roughness is desired on the left edge. RMS is determined using equation 4.1 for the left edge of the angled strut which is produced using simulation result. Orthogonal array similar to Table 10 is constructed to determine the signal noise ratios. Based on the response plot for main effects, the optimized factor levels are determined for left edge of angled struts.

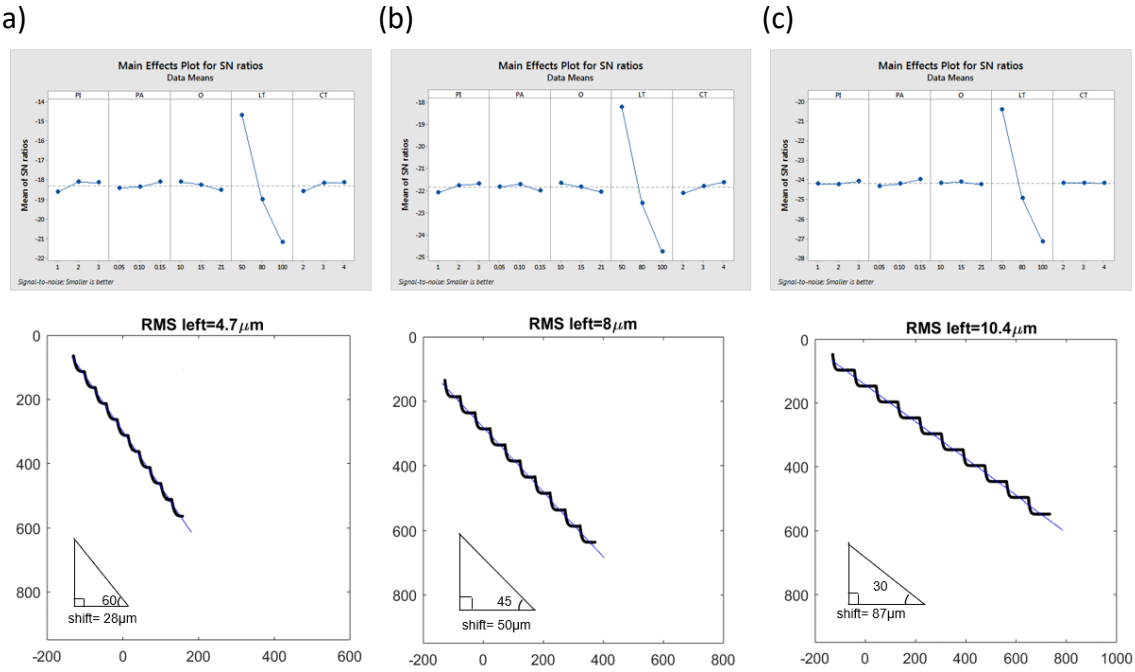

Figure 4.14 Optimization of printing parameters when left edge is critical to quality (a) Inclination angle=60°, (b) Inclination angle=45° and, (c) Inclination angle=30°

From Figure 4.14, it is seen that layer thickness is the primary factor that affects the surface roughness. As the layer thickness will influence the shift distance, it will be the primary factor to be optimized that will lead to high-quality angled strut irrespective of edges that are critical to quality. Printing parameters [PI], [PA], and [O] contribute in quality improvement by suggesting higher [PI], lower [PA] and lower [O] along with lower layer thickness will result in high-quality structure.

Second, right edge is selected critical to quality. Since this edge will not have the overlapping effect due to top layer, it will be rougher. Figure 4.15 shows the response plots and surface roughness for right edge of the angled struts. If this edge is critical to quality, the important factor other than the printing parameters is the inclination angle. Higher inclination angle and lower layer thickness will result into lower shift distance, thereby producing a high-quality strut.

(a) (b) (c)

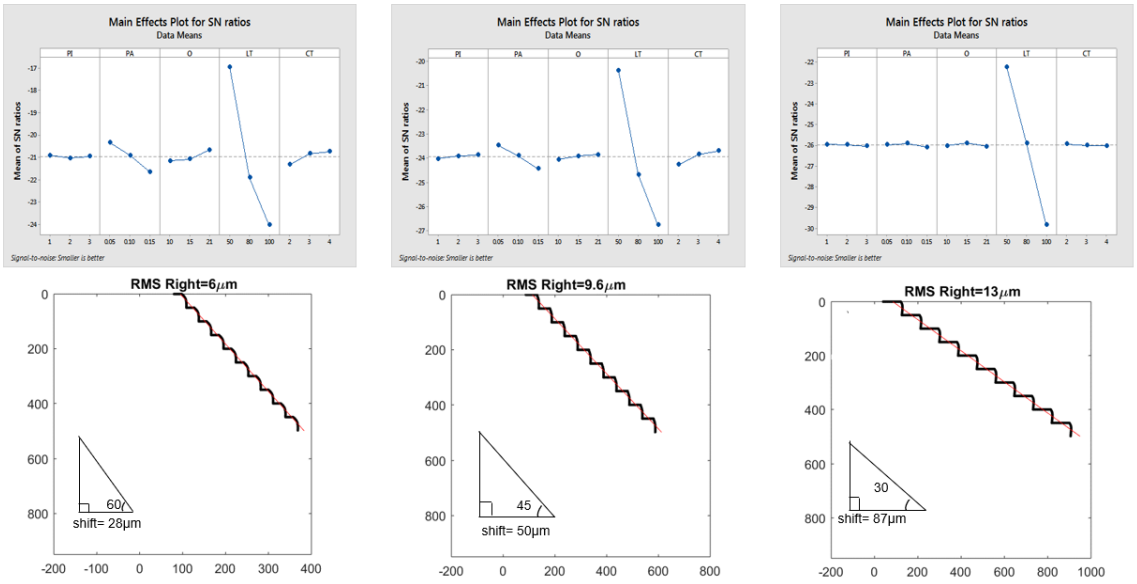

Figure 4.15 Optimization of printing parameters when right edge is critical to quality (a) Inclination angle=60°, (b) Inclination angle=45° and, (c) Inclination angle=30°

The third case is for a strut where both edges are critical to quality. For this case the RMS for left edge and right edge are the responses. Due to this, the orthogonal array will have two columns that represent the noise. Using 'smaller the better' formula for determining optimal factor levels, the main effects plot is constructed. From Figure 4.16, it is evident that for different inclination angles, layer thickness is the primary factor that affects the surface roughness. Angled struts with inclination of 45° and 60° have

optimized factor levels similar to vertical struts, therefore it is assumed that same optimized factors will lead to an overall high-quality structure.

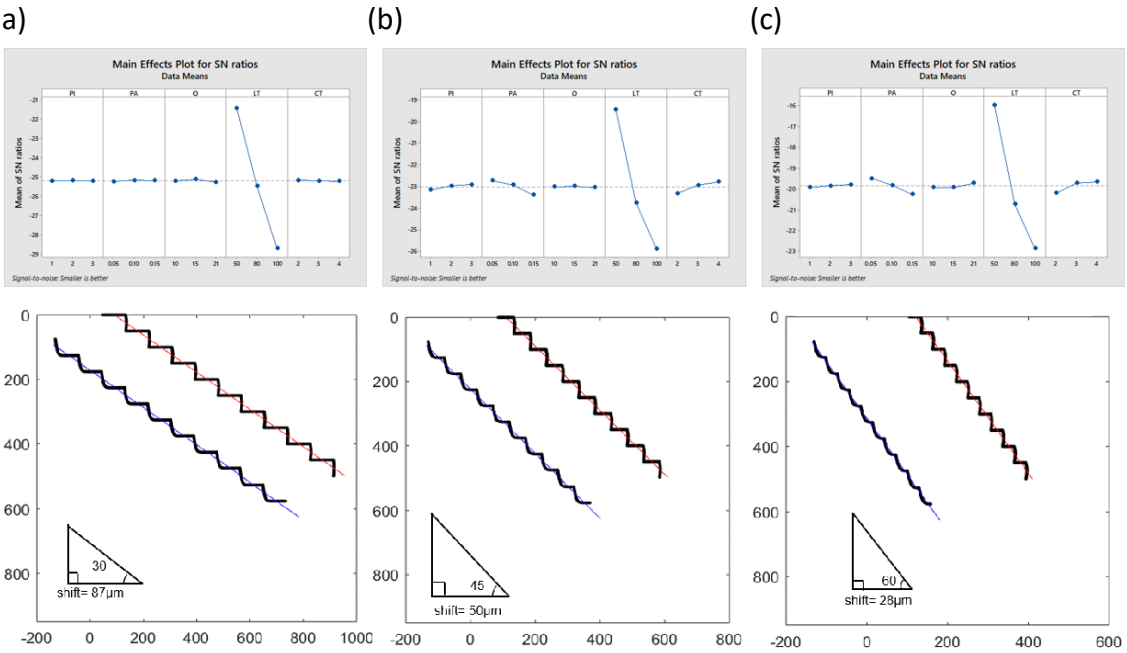

Figure 4.16 Optimization of printing parameters when both edges are critical to quality (a) Inclination angle=30°, (b) Inclination angle=45° and, (c) Inclination angle=60°

Table 12 Inclined strut RMS

Inclination Angle (°)	Left edge RMS (µm)	Right edge RMS (µm)
30	10.3	13.3
45	7.6	10.3
60	4.6	7.5

When the 60° inclined strut is compared with the nominal parameters (same as used in Case 1), it is clear that the surface roughness is reduced by selecting optimal parameters. The Figure 4.16 shows the strut with nominal parameters and their RMS. The surface topography of left edge of the optimized inclined strut, when compared with nominal inclined strut, is improved by approximately 45%. The surface topography

of right edge of the optimized inclined strut is improved by approximately 34%. This method will reduce dependency on post-processing required for inclined strut.

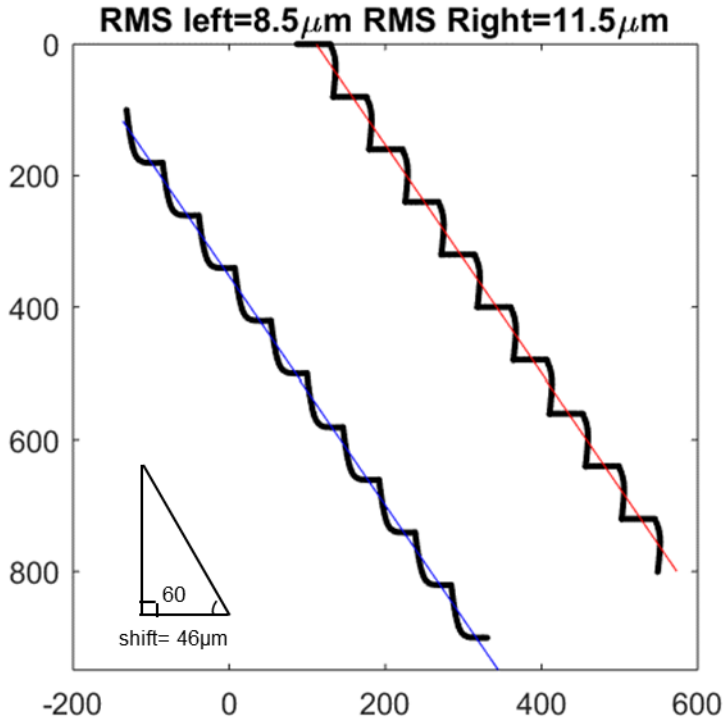

Figure 4.17 Surface topography of 60° inclined strut with nominal parameters showing decrease in quality

For inclined struts, the time-quality tradeoff will have a larger scope. Since printing structures with large layer thickness make them relatively rough and easier to break , it is recommended to use the Taguchi's optimized thickness. However, if the layer thickness needs to be sacrificed, it is advisable to follow the optimized parameters that will ensure high conversion due to high [PI], thicker and firmer profile due to low [PA] (since the cured layer overlapping on lower layer will be dominant), moderate oxygen concentration to allow minimal tacky layer formation for increasing interfacial strength between two layers [9] and Taguchi estimated curing time to potentially establish optimized high-quality strut.

5 Conclusion and Future Work

5.1 Conclusion

In this work, a computational model representing the photopolymerization principle was presented that simulates the 3D printing environment. The primary purpose of this model is to analyze how varying resin parameters affect 3D printing. Secondly, the model is used to program 3D printed structures to optimize the print-process parameters.

A detailed experimental analysis of parameters is performed to study their effect on the cure depth and cure width. These results when compared with mathematical model, determine the conversion ratio cut off and layer profile. From experimental and simulation data, the conversion ratio cut off from HDDA was found out to be 4%. The simulation model also determined the effect of photopolymerization on resin species such as the monomer, radicals, [PI], [PA] and [O]. The validation allowed to recognize the potential of the model to develop high quality 3D printed structures.

Pre-processing the resin parameters to obtain high-quality structures was the challenge addressed through validated model. Since, mere evaluation is unable to suggest parameters for the high-quality structures, design of experiments concept was introduced. Taguchi's Orthogonal Array Method was used to select the optimized parameters that would improve the quality of 3D printed structure, which is characteristically represented by minimum surface roughness or RMS.

Vertical micro-struts are printed with optimum parameters and compared with the result obtained with nominal parameters. The result shows that the optimized

parameters reduce surface roughness by 40%. Utilizing the optimized printing parameters requires the use of small layer thickness, which affects total print time. To address this trade off, the Orthogonal Array can be investigated to select the experiment number which will allow relaxed use of layer thickness but still maintain a minimum surface roughness value. Varying printing parameters such as [PI], [PA] and [O] will not influence print time, thereby allowing them to influence the surface roughness. It is seen that [PI] increment, [PA] and [O] decrement will still allow to lower the surface roughness even if layer thickness is large, thereby allowing to lower total print time for large samples.

Based on this trend, optimized factor levels from Taguchi OA were used to study inclined struts. For inclined struts, the variance of surface profiles on the edges were studied and the requirement to study RMS for both edges was established. The effect of inclination angle on surface topography shows higher inclination will give minimum roughness. With the optimized parameters, surface roughness of the inclined strut decreases by 45% for left edge and 34% for right edge when compared to the part with nominal parameters. Time-quality trade off was discussed and the overlapping effect of layers was used as an advantage to minimize surface roughness by choosing larger layer thickness and optimized printing parameters.

In conclusion, surface topography of a vertical or inclined 3D printed strut can be improved by optimizing the print process parameters using the mathematical model and Taguchi method, and high-quality parts can be manufactured by reducing post-processing cost and time.

5.2 Future Work

As expressed above, the possible future work is to establish a model that is more sensitive towards cure width thereby able to reduce the gap between experimental and simulation RMS values. This can be done by performing elaborate experiments to obtain the constants for the simulation purpose rather than performing iterative approach to finalize their values.

Also, temperature related analysis can be included in the simulation to study the effect of heat generation on conversion ratio. The effect of varying kinetic constants can also be established by doing elaborate experimentation. Further, a powerful computer can be used to establish a simulation for higher meshing and more accuracy.

Lastly, the layer profile analysis can be performed by creating different shapes of struts and estimating the surface roughness values and their effect if the 3D part to be printed is sliced in a different orientation.

References

[1] Mohammad Vaezi, Hermann Seitz, Shoufeng Yang (2012), 'A review on 3D micro-additive manufacturing technologies', Int J Adv Manuf Technol (2013), DOI 10.1007/s00170-012-4605-2

[2] Young Myoung Ha, Jae Won Choi and Seok Hee Lee, 'Mass production of 3-D microstructures using projection microstereolithography', Journal of Mechanical Science and Technology (2008), 22, 514-521

[3] Xiaoyu Zheng, Joshua Deotte, Matthew P. Alonso et al., 'Design and optimization of a light-emitting diode projection micro-stereolithography three-dimensional manufacturing system', Review of Scientific instruments (2012), 83, 125001-6

[4] Tryson G. R. and Shultz, A. R., 'A Calorimetric Study of Acrylate Photopolymerization', Journal of Polymer Science: Polymer Physics Edition (1979), v17, 2059-2075

[5] N. Fang, C. Sun and X. Zhang, 'Diffusion-limited photopolymerization in scanning-micro-stereolithography', Applied Physics (2004), A 79, 1839-1842

[6] Christian Decker and Aubrey D. Jenkins, 'Kinetic Approach of O2 Inhibition in Ultraviolet- and Laser-Induced Polymerizations', Macromolecules (1985), 18, 1241-1244

[7] Allison K. O'Brien et al., 'Impact of oxygen on photopolymerization kinetics and polymer structure', Macromolecules (2006), 39, 2501-2506

[8] D. Dendukuri, P. Panda, R. Haghgooie, Ju Min Kim, T. Alan Hatton, and Patrick S. Doyle, 'Modeling of Oxygen-Inhibited Free Radical Photopolymerization in a PDMS Microfluidic Device', Macromolecules (2008), 41 (22), 8547-8556

[9] Zeang Zhao, Xiaoming Mu, Jiangtao Wu, H. Jerry Qi, Daining Fang, 'Effects of oxygen on interfacial strength of incremental forming of materials by photopolymerization', Extreme Mechanics Letters (2016), 9, 108-118

[10] Xi, 'Chapter 2: Numerical Simulation of micro-scale photopolymerization', MS Thesis (2015)

[11] Amit S. Jariwala, F. Ding, A. Boddapati, V. Breedveld, M. A. Grover, C. L. Henderson, and D. W. Rosen, 'Modeling effects of oxygen inhibition in masked-based stereolithography', Rapid Prototyping Journal, (2011), 17 (3), 168-175

[12] Daekeon Ahn, Hochan Kim and Seokhee Lee, 'Surface Roughness prediction using measured data and interpolation in layer manufacturing', Journal of Materials Processing Technology (2009), 209, 664-671

[13] Benay Sager, David W. Rosen, 'Use of parameter estimation for stereolithography surface finish improvement', Rapid Prototyping Journal (2008), 14 (2), 213-220

[14] Daehoon Han, C. Farino, Chen Yang, T. Scott, D. Browe, W. Choi, J. W. Freeman and Howon Lee, 'Soft Robotic Manipulation and Locomotion with a 3D Printed Electroactive Hydrogel', ACS Appl. Mater. Interfaces (2018), 10 (21), 17512-17518

[15] George Odian, 'Principles of Polymerization: Fourth Edition', John Wiley & Sons Inc (2004)

[16] Jiangtao Wu, Zeang Zhao, Craig M. Hamel, X. Mu, X. Kuang, Z. Guo and H. Jerry Qi, 'Evolution of material properties during free radical photopolymerization', Journal of Mechanics and Physics of Solids (2018), 112, 25-49

[17] Howon Lee, 'Three-dimensional micro fabrication of active micro devices using soft functional materials', UIUC, Dissertation, (2011)

[18] K. K. Rohatgi-Mukherjee, 'Fundamentals of Photochemistry', New Age International (P) Ltd., Publishers (1978)

[19] Ian Gibson, David Rosen, and Brent Stucker, 'Additive Manufacturing Technologies: 3D Printing, Rapid Prototyping, and Direct Digital Manufacturing 2nd ed.', Springer. ISBN 978-1-4939-2112-6

[20] Ciba Specialty Chemicals, 'Manual for Photoinitiators for UV curing' (2003)

[21] Trelleborg sealing solutions, 'Aerospace Engineering Guide' (2008)

[22] Benjamin Lee, 'Introduction to 12 Degree Orthogonal Digital Micromirror Devices (DMD)', Texas Instruments, (2008)